STUDY ON THE DEVELOPMENT

OF AXIAL STRESSES IN WOUND ROLLS

By

ANGELA DE'ON WELCH

Bachelor of Science in Mechanical Engineering

Oklahoma State University

Stillwater, OK

2006

Submitted to the Faculty of the
Graduate College of the
Oklahoma State University
in partial fulfillment of
the requirements for
the Degree of
MASTER OF SCIENCE
December, 2006

STUDY ON THE DEVELOPMENT

OF AXIAL STRESSES IN WOUND ROLLS

Thesis Approved:

J. K. Good

Thesis Adviser

D. E. Fisher

C. E. Price

A. Gordon Emslie

Dean of the Graduate College

TABLE OF CONTENTS

LIST OF TABLES

Table Page

LIST OF FIGURES

LIST OF SYMBOLS AND ABBREVIATIONS

PET	Polyester Film
WHRC	Web Handling Research Center
HSWL	High Speed Web Line
MD	Machine Direction
CMD	Cross Machine Direction
pli	pounds per linear inch
fpm	feet per minute
E_r	Radial Young's modulus
E_θ	Tangential Young's modulus
σ_r	Radial stress
σ_θ	Tangential stress
σ_z	Axial stress
ε_r	Radial strain
ε_θ	Tangential strain
ε_z	Axial strain
r	Radius
d	Diameter
$\nu_{r\theta}$	Poisson's ratio of stress in θ-direction to strain in r-direction
$\nu_{\theta r}$	Poisson's ratio of stress in r-direction to strain in θ-direction
ν_{zr}	Poisson's ratio of stress in r-direction to strain in z-direction

$\nu_{\theta z}$	Poisson's ratio of stress in z-direction to strain in θ-direction
P	Normal pressure
K_1	Material constant
K_2	Material constant
δ_{ij}	Level of interference
u_i, u_j	Nodal points
T_w	Web tension
t	Web thickness
w	Web width
α	Reinforcement factor
R_{outer}	Outer radius of core
G_{rz}	Shear modulus
Y	Distance of neutral axis
R	Radius of curvature
$\varepsilon_\theta(r)$	Tangential strain at certain radius, r
$\varepsilon_z(r)$	Axial strain at certain radius, r
ε_θ(gage)	Tangential strain at gage's radius
ε_z(gage)	Axial strain at gage's radius

CHAPTER I

INTRODUCTION TO STRESSES IN WOUND ROLLS

Web materials are very common in manufacturing environments today and will continue to be in the future. A web is defined as a material whose length is much greater than its width and whose width is much greater than its thickness. Webs can be made of just about anything. Several common categories of web materials include paper, plastic films, metal foils and laminates. Hundreds of thousands of products are made from these webs and webs encompass many of the products used in daily life. In manufacturing environments, wound rolls of web material are often the most economical and practical solution for material storage and transportation.

Unfortunately, this is not without several problems. Just the act of winding the web can cause damage of several kinds to the web. This damage has been the topic of numerous research studies. The quality of the wound roll depends on the stresses which exist in it. While these in-roll stresses determine the structural integrity of the roll, they can also impart damage onto the roll. If these stresses are allowed to go uncontrolled, the results are tearing and buckling along with many other defects in the wound material.

This study focuses on the exploration of stresses that induce corrugation failures. Corrugations can occur axially or circumferentially, but this study focuses on circumferential corrugations only. Circumferential corrugations are buckles that form circumferentially about wound rolls as the result of axial stresses. If the corrugations become too large in amplitude, a burst, which is a complete fracture of the web, may result. Many webs are viscoelastic and rolls with corrugations within will creep through time. When the web is unwound as it enters the next manufacturing process, baggy lanes will be seen in the free web spans at the same lateral location as the corrugations. Coating and printing operations will become difficult and finally not possible depending on the degree of bagginess. A picture of circumferential corrugations in a wound roll of polyester web is shown in Figure 1.

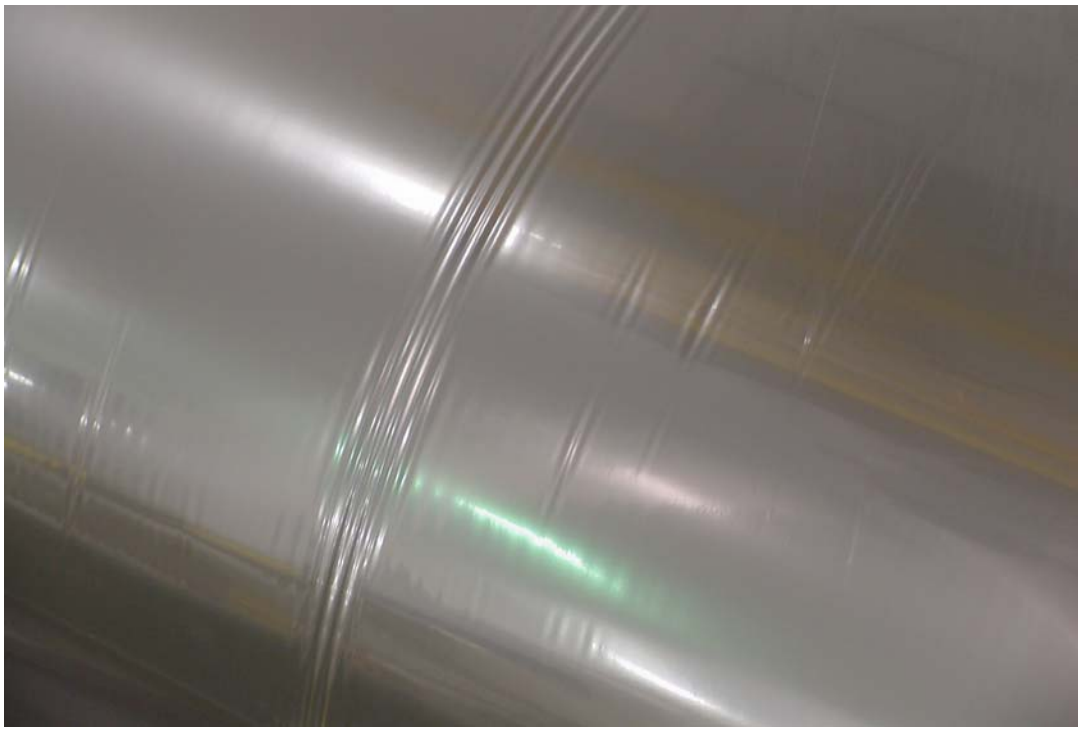

Figure 1: Circumferential Corrugations

Many studies have been done which focus on such defects, but not many studies relate the defects to the wound roll models. Using winding models is an excellent way to predict wound roll defects. With the increasing complexity of such winding models, more accurate prediction of defects is becoming possible.

The winding process is not the sole source of stress in wound rolls. There are other factors that create axial stresses in the roll including thermal, moisture and absorption, and viscoelasticity. For this particular study, only stresses due to winding will be evaluated. The winding stresses in the roll are produced by winding tension. The winding tension is applied to the web as it is being wound. If these stresses are known to be a function of winding tensions, then the stresses can be predicted and defects can be avoided. Most of the research done has focused on stresses as a function of web tension.

The study of the stresses in a wound roll of material has sparked various research studies and produced several one-dimensional models to aid in predicting when stresses will occur. The one-dimensional models have typically been written as differential equations written in terms of radius, radial pressure, and material considerations. The material considerations are usually given a plane stress treatment. Models written in this form have little value here since plane stress involves an assumption of zero axial stress. A few plane strain models have been developed which allow a non-zero axial stress, but enforce a zero axial strain constraint. The wound roll is neither a consideration of plane stress or plane strain. The web approaches the winder as a membrane subject to tension in the direction of travel (called the machine direction). There is a negative strain in the cross machine direction, due to the Poisson's effect, which becomes the axial direction as

the web is wound into a roll. Thus, wound rolls are not situations of plane stress or plane strain.

While one-dimensional models are somewhat helpful, two-dimensional models can help with further predictions. Two-dimensional, axisymmetric models have been developed which require no assumption of material consideration. A two-dimensional model will be used in this study.

The experimental portion of this study was conducted in the labs of the Web Handling Research Center at Oklahoma State University. The WHRC is an industry/university cooperative research center and was sponsored in part by the National Science Foundation during the initial years. The WHRC has now been in operation for 20 years and is the only center of its type in the world, so any research done there is very important to the industrial sponsors. The WHRC houses many different types of winders, but the High Speed Web Line will be used for the experimental portion of this study. The HSWL is capable of running a 30 inch wide web at speeds of up to 5000 ft. per minute, although this speed will not be approached in this study. The HSWL can hold and retain web tension, even at zero velocity, which is important for the current study. Figure 2 shows a picture of the winding and unwinding sections of the HSWL where the experimental portion will take place.

Figure 2: Experimental Area of High Speed Web Line

While some research has been done on axial stresses, there is much more to be discovered. The topic of this thesis study is the development of axial stresses in wound rolls. The axial stresses will be calculated using a two-dimensional winding model. Those stresses will be used to compute strains that will be verified experimentally. The reason for conducting this study is to determine if the axial stresses that are associated with winding are sufficient to cause corrugation failures.

CHAPTER II

BACKGROUND INFORMATION

Winding models exist so that predictions about a wound roll of web can be studied in more detail. The simplest of these models is a one-dimensional model. The main purpose of a one-dimensional model is to predict how stresses in the wound roll behave as a function of radius [5]. A more complex prediction is completed with the use of a two-dimensional model. Two-dimensional models can predict cross machine direction (CMD) stresses as well as the machine direction (MD) stresses that one-dimensional models can predict. Both types of model are researched in this chapter.

Forrest [6] lists the typical factors of roll defects as winding tension, web thickness and material properties. These factors, as well as provisions for entrained air and methods, were used to predict the formation of common roll defects. The buckling criteria are further developed to predict deformations induced by axial and circumferential stresses, resulting in radial pressures and circumferential and axial direction stresses for the plane strain situation.

One-Dimensional Winding Models

Before discussing research related to a two-dimensional winding model, like the one used in this study, a one-dimensional model will be discussed. There were several assumptions that were made with a one-dimensional model as stated by Hakiel [1]. The first assumption was that the winding roll was treated as a geometrically perfect cylinder where the web was assumed to have perfectly uniform thickness, width, and length. The roll was also assumed to be a collection of concentric hoops of web and not a spiral. The winding process itself was modeled as an incremental process of adding "tensioned hoops of web" onto the roll. As each layer is added, the elastic properties of that layer were assumed to remain constant, but not necessarily the same constant values that exist in other layers. This is important because the radial modulus of a wound roll has been shown to be state dependant on the contact pressure between the web layers. The pressure in the wound roll can vary with radius and thus the radial modulus will vary with radius. In a one-dimensional model the stresses (σ_r, σ_θ, and σ_z for plane strain) are assumed to be functions of radius (r). The roll is assumed to be an orthotropic, elastic cylinder and yet another assumption stated that the stresses in the wound roll were assumed to be functions of the radius, but not of axial or circumferential position. The final assumption stated that plane stress conditions were in effect, which is shown mathematically, in the following equations [11]:

$$\varepsilon_r = \frac{\sigma_r}{E_r} - \frac{\upsilon_{r\theta} \cdot \sigma_\theta}{E_\theta} \quad , \tag{2.1}$$

$$\varepsilon_\theta = \frac{\sigma_\theta}{E_\theta} - \frac{\upsilon_{\theta r} \cdot \sigma_r}{E_r} \quad , \tag{2.2}$$

where E_r and E_θ are the radial and tangential Young's moduli, $\upsilon_{r\theta}$ is Poisson's ratio of the impact of a stress in the θ-direction to the strain in the r-direction, and $\upsilon_{\theta r}$ is Poisson's ratio of the impact of a stress in the r-direction to the strain in the θ-direction.

The strain compatibility equation could be derived from the linear symmetric definitions of small axisymmetric strains. These definitions are shown below:

$$\varepsilon_r = \frac{du}{dr} \qquad \varepsilon_\theta = \frac{u}{r}, \tag{2.3 and 2.4}$$

Equation 2.4 can be manipulated to show the following:

$$u = \varepsilon_\theta \cdot r, \tag{2.5}$$

At this point, Equation 2.5 can be substituted into Equation 2.3 to show the following:

$$\varepsilon_r = \frac{d\varepsilon_\theta}{dr} \cdot r + \varepsilon_\theta, \tag{2.6}$$

Finally, the strain compatibility equation can be found by manipulating Equation 2.6, as shown below:

$$r\left(\frac{d\varepsilon_\theta}{dr}\right) + \varepsilon_\theta - \varepsilon_r = 0, \tag{2.7}$$

The compatibility equation for stress can be found in a similar way, resulting in the following equation:

$$r\left(\frac{d\sigma_r}{dr}\right) + \sigma_r - \sigma_\theta = 0, \tag{2.8}$$

where σ_r and σ_θ are stresses in the radial and tangential directions.

The second-order linear differential equation in terms of radial stress could now be found. The two compatibility equations (Equation 2.7 and Equation 2.8) were set

equal to one another and then manipulated and rearranged using the definitions for radial and tangential strain (Equation 2.1 and Equation 2.2) to get the following:

$$r^2\left(\frac{d^2\sigma_r}{dr^2}\right) + 3r\left(\frac{d\sigma_r}{dr}\right) - \left(\frac{E_\theta}{E_r} - 1\right)\cdot\sigma_r = 0 \quad , \tag{2.9}$$

At this point, the core boundary condition and the outer layer boundary condition were needed which were related to σ_r, but as layers were added, the two boundary conditions may change. The radial modulus, E_r, may be changing as a function of the pressures at the various winding radii, but these models were series solutions and did not require layer by layer solutions.

One-dimensional models begin to differ after the above assumptions. One model, produced by Catlow et al. [7], made the assumption that a wound roll could be modeled as a linear isotropic material. In other words, the radial modulus and the circumferential modulus of elasticity were equal (E_r=E_θ). Another one-dimensional model, produced by Altmann [8] and Yagoda [9], made the assumption that a wound roll could be modeled as a linear anisotropic material, so the radial modulus of elasticity was not equal to the circumferential modulus of elasticity, although both were constants. A benefit of E_r and E_θ being constants, but not necessarily equal, was that a reverse model could be produced. The reverse model would solve for the profile in winding tension as a function of wound roll radius that would yield a profile in radial pressure [13]. Therefore, if it was known prior to winding that a certain profile in radial pressure was desirable; the reverse model would prove to be quite useful. Hakiel [1], after defining a method for computing the stress distributions in a winding roll for a single lap, then computed the total stress distribution for the wound roll by solving a set of equations to compute the stress for each

lap wound and then added all the laps together. He found that the pressure predicted by the linear model was proportional to the intensity of the winding tension.

Cole and Hakiel [2] conducted a study in which the roll was partitioned in the widthwise direction into a discrete number of segments. Within each segment, process parameters, the stresses and the displacements were width dependant. The theoretical stresses and displacements within the segments were calculated using an algorithm used by Hakiel in an earlier experiment. The experimental part of the study was performed by instrumenting two strain gages onto each segment of the core of the roll to measure the circumferential contraction of the segment. Pressure readings were obtained with the segmented, instrumented core. During the winding process, the winder was stopped several times, while the tension was maintained, so that measurements of pressure at the core could be performed. The pressure could be compared to the radial stress predicted by the model at the radial location of the core. The experimental method of Hakiel's study showed similarities to the experimental portion of this study as described in Chapter 4.

The output of these models was radial and circumferential stress as a function of radius (σ_r and σ_θ) and the radial location of layers, sector by sector. Each sector was assumed to exist in a plane stress condition. Thus, axial stress output was not possible since all axial stresses (σ_z) were assumed to be zero. This model is mentioned here since it was one of the first two-dimensional models to be introduced. Kedl [4] introduced a similar model in the same time frame.

Pfeiffer [12] showed a relationship between pressure versus strain and modulus versus pressure. The radial modulus is a state dependent parameter which includes

structural and material nonlinearities. Asperities on the surface of a wound or stacked web contact the asperities of the next surface and so on. When compressing the surface of the web, and sometimes the internal contact area, the strain becomes a function of radii or normal pressure and the measured radial modulus of elasticity, E_r, is now a function of radial stress. When speaking of stresses, the common sign convention is positive for tensile stresses and negative for compressive stresses. When speaking of wound rolls, a tensile radial stress would make no sense, resulting in a separation of the layers. In this case, the tensile radial stress is replaced with pressure by omitting the sign.

Pfeiffer found the relation between normal pressure and normal strain to be logarithmic in form per the following equation, also known as the Pfeiffer Equation:

$$P = -\sigma_r = K_1\left(e^{K_2 \cdot \varepsilon_r} - 1\right) \quad , \tag{2.10}$$

which makes the radial modulus of elasticity:

$$E_r = \frac{d\sigma_r}{d\varepsilon_r} = K_2\left(P + K_1\right) \quad , \tag{2.11}$$

where K_1 and K_2 are determined experimentally, by curve fitting pressure versus strain data collected from stack compression tests.

More relationships between the material constants and stress and strain were made by other researchers. Willett and Poesch [10] used a polynomial to represent the radial modulus. In stack tests, ε_r and ε_θ were measured in an attempt to measure Poisson's Ratio as in the following equation:

$$\upsilon_{\theta r} = \frac{-\varepsilon_r}{\varepsilon_\theta} \quad , \tag{2.12}$$

Equation 2.12 is simply a reduction of Equation 2.2 and assumes that $\sigma_\theta=0$. Willett and Poesch [10] discovered that $\nu_{\theta r}$ varied with pressure, but then assumed that its value was constant for reasons undisclosed in the research.

The only measurements of $\nu_{\theta r}$ have been from Willett and Poesch and from Good and Markum [5]. The radial strain was fairly easy to measure in a compression test, but the tangential strain was not so easily measured. The stack tests conducted by Good and Markum showed that the following equation may be valid at high pressures for stacks.

$$\frac{\upsilon_{r\theta}}{E_\theta} = \frac{\upsilon_{\theta r}}{E_r} \quad , \tag{2.13}$$

The above equation is also known as Maxwell's Equation [5] and is widely accepted for many paper, plastic, and foil webs where the in-plane modulus, E_θ, is constant and the radial modulus, E_r, is state dependent on the radial stress, σ_r, which make Poisson's Ratio state dependent on pressure. The output of one-dimensional plane stress models was largely unaffected by Poisson's ratios ranging from 0.01 to 0.5. However, axial stresses in two-dimensional models are sensitive to the Poisson's Ratios $\nu_{r\theta}$, ν_{rz}, and $\nu_{\theta z}$. This sensitivity to Poisson's Ratio will be discussed further.

As mentioned previously, Good and Markum [5] conducted stack compression tests on polyester films to verify that $\upsilon_{\theta r}$ was in fact state dependant on pressure. The use of one-dimensional wound roll models indicated the impact of varying the input of Poisson's Ratio was small on the internal stresses produced within the wound roll. This was particularly important, since these Poisson's Ratios are so hard to measure experimentally. The tests consisted of adhering strain gages to the film's surface in the tangential direction and the strain in the normal direction, ε_r, was measured and controlled during the test. With the two measured strains, the Poisson's Ratio, $\upsilon_{\theta r}$, could

be inferred using Equation 2.12 at various pressure levels. Using this method, it appeared $\upsilon_{\theta r}$ was dependant on radial stress and approached a value of 0.01. While it is generally accepted that $\upsilon_{r\theta}$ is constant for film webs and is in the range of 0.3-0.4, it would govern the thinning of the web when subjected to tension in the tangential direction.

The one-dimensional winding models that were discussed in this chapter produce outputs such as radial pressure and the circumferential stress as a function of radius. While these models are useful for showing the number of roll defects in narrow rolls, where the pressures and circumferential stresses are uniform across the small width of the roll, a two-dimensional model is more helpful for wider rolls or on rolls where pressures and circumferential stresses are not uniform.

Since most webs are nearly impossible to produce with a constant thickness, the need began to arise for a model that could predict how the internal stresses vary with respect to the radius and CMD location. While the variation in web thickness could be caused by a number of different factors, it is not possible at this time to resolve this issue, so two-dimensional models are used to aid in predictions of roll defects.

Two-Dimensional Winding Models

Two-dimensional models take the web thickness, profiled in the CMD and the web width, separated into segments [11]. Each segment would be assigned a web thickness and a one-dimensional model would be used to evaluate that particular segment. The models were limited to center winding, but it is the allocation of web tension across the web width that is the key point for these models. The sum of all the tensions in each segment across the width is equivalent to the total web tension in the winder tension zone.

Lee and Wickert [3] developed a model for predicting the stress field within a wound roll in which radial, circumferential, axial and shear stresses could vary in the radial and axial directions. A key assumption in the one-dimensional models was the specification that core stiffness must be uniform across the roll's width. This restriction was re-examined in the two-dimensional analysis. The widthwise variation of stresses in wound rolls were investigated using a two-dimensional, axisymmetric, finite element model. The wound roll was separated into two regions: the core and the layered web substructures. The general core geometry and designs were accommodated, analyzed, and optimized. The axial and shear stress were significant only near the core-web interface and were attributed to Poisson coupling and strain mismatch between material properties. The model developed could be used for quantifying stress concentration at the edges of the core-web interface. The research described will be furthered to include investigation of the stress state in the presence of non-uniform winding tension or material thickness across the web's width.

Kedl [4] described a model for estimating the stresses throughout a wound roll as a function of both radius and width. The model computed the effects of CMD non-uniformity by dividing the roll into an arbitrary number of CMD segments, treating each as a separate roll with its own winding tension. In order to compute the tension, segment diameters were determined by using a special model based on stacking thick walled cylinders with orthotropic properties. Calculations of the wound-in pressure and tension were computed from any existing model that allowed the compressive roll modulus to be a function of pressure. The experimental results obtained in this study showed that the

model adequately predicted the center wound roll as a function of cross-web caliper variation over the web width.

Hoffecker and Good [11] developed a two-dimensional model that employed an axisymmetric finite element method. A series of quadrilateral elements were used to model a layer, or group of layers, in the wound roll. The web thickness was allowed to vary linearly across the width of each quadrilateral. The primary output of finite element codes in solid mechanics were nodal deformations. Strains and stresses were secondary outputs since they depend on the knowledge of the deformation of the finite elements. This particular model was used for the study at hand and will be discussed further in Chapter 3.

The outputs of two-dimensional models differ slightly from the one-dimensional models. Two-dimensional models are able to output radial pressure, circumferential stress, axial stress, and shear stress as a function of the axisymmetric location. Roll deformation can also be calculated across the roll width. Defects predicted with the two-dimensional models are more accurate than the defects predicted with the one-dimensional models, assuming that all of the needed information is available to provide the two-dimensional models.

The winding models discussed in this chapter are a good starting point to predict wound roll defects, but the winding models that predict axial stresses have never been verified, which leads to one of the research objectives of this study. Verification will be obtained by comparing the magnitude of circumferential and axial strains that form in wound rolls by two-dimensional winding models as well as lab experiments. The stresses will be evaluated to see if they are sufficient to cause corrugations.

CHAPTER III

DISCUSSION ON TWO-DIMENSIONAL WINDING MODEL AND APPLICATION TO THE POLYESTER WEB TO BE TESTED

As introduced in Chapter 2, the winding model used in the verification portion of this study was developed by Hoffecker and Good [11]. The model used an axisymmetric finite method in which a series of quadrilateral elements were used to model a layer, or group of layers, in a wound roll. The model analyzed an orthotropic core or will accrete/wind a three-dimensional roll. As each layer was accreted onto the outside of the roll, the new outside radius was part of the primary solution vector.

There were a few critical steps involved in determining the stiffness of a four-node axisymmetric, quadrilateral element. In webs that are a few thousands of an inch thick, like the one used in the current study, only the membrane stresses are important within a given layer. The membrane stresses are constant throughout the thickness of a given layer. The deformations for a four-node axisymmetric quadrilateral are as follows:

$$\begin{pmatrix} u \\ w \end{pmatrix} = \begin{pmatrix} N_1 & 0 & N_2 & 0 & N_3 & 0 & N_4 & 0 \\ 0 & N_1 & 0 & N_2 & 0 & N_3 & 0 & N_4 \end{pmatrix} \cdot \begin{pmatrix} u_i \\ w_i \\ u_j \\ w_j \\ u_k \\ w_k \\ u_l \\ w_l \end{pmatrix}, \tag{3.1}$$

where the shape functions, N_i, are as follows [14]:

$$\begin{pmatrix} N_1 \\ N_2 \\ N_3 \\ N_4 \end{pmatrix} = \begin{bmatrix} \frac{1}{4}\cdot(1-\xi)(1-\eta) \\ \frac{1}{4}\cdot(1+\xi)(1-\eta) \\ \frac{1}{4}\cdot(1+\xi)(1+\eta) \\ \frac{1}{4}\cdot(1-\xi)(1+\eta) \end{bmatrix}, \tag{3.2}$$

These shape functions are an adequate representation for modeling near constant values of stress and strain throughout a given element.

Orthotropic materials have three mutually perpendicular planes of elastic symmetry. The model used for the current study analyzes the material as orthotropic. The constitutive equations for an orthotropic three-dimensional axisymmetry material are shown in the following matrix of equations [14]:

$$\begin{pmatrix} \varepsilon_r \\ \varepsilon_\theta \\ \varepsilon_z \\ \gamma_{rz} \end{pmatrix} = \begin{pmatrix} \frac{1}{E_r} & \frac{-\upsilon_{\theta r}}{E_\theta} & \frac{-\nu_{zr}}{E_z} & 0 \\ \frac{-\nu_{r\theta}}{E_r} & \frac{1}{E_\theta} & \frac{-\nu_{z\theta}}{E_z} & 0 \\ \frac{-\nu_{rz}}{E_r} & \frac{-\nu_{\theta z}}{E_\theta} & \frac{1}{E_z} & 0 \\ 0 & 0 & 0 & \frac{1}{G_{rz}} \end{pmatrix} \cdot \begin{pmatrix} \sigma_r \\ \sigma_\theta \\ \sigma_z \\ \tau_{rz} \end{pmatrix}, \qquad (3.3)$$

Maxwell's Equations, shown below, are also important in the development as the ε_z and ε_θ strains are affected by all the stresses (σ_r, σ_θ, and σ_z) through Poisson's Ratios that are not known well.

$$\frac{\nu_{\theta r}}{E_\theta} = \frac{\nu_{r\theta}}{E_r} \qquad \frac{\nu_{zr}}{E_z} = \frac{\nu_{rz}}{E_r} \qquad \frac{\nu_{\theta z}}{E_\theta} = \frac{\nu_{z\theta}}{E_z}, \qquad (3.4, 3.5, 3.6)$$

It was previously stated that, according to Good and Markum, the Poisson's Ratio, $\nu_{\theta r}$, varied and it is assumed here that the Poisson's Ratios, $\nu_{r\theta}$ and ν_{rz}, vary as well. It is not easy to measure these values, as Good and Markum reported, but an adequate approximation could be made for this study. An explanation of this approximation is discussed later in this chapter.

Material Properties

Before the results of the two-dimensional analysis can be described, the web material and core material used in the analysis will be reported. The web material used was a polyester film (PET) in two different widths, 6 inch and 24 inch. Two widths were tested in the hope that near plane stress conditions would exist in the 6 inch width case and perhaps a condition approaching plane strain would exist for the 24 inch width web. The core material used for winding was made of steel, with an outside diameter of 3.8

inches and an inside diameter of 3.0 inches. The web material and core material properties listed in Table 1 were needed to report to the model for the code to run. The winding tension of 2.0 pli for the 6 inch wide web and a corrected winding tension value of 2.04 pli for the 24 inch wide web were also needed to input to the code and is also shown in Table 1.

Web Material Properties		**Core Material Properties**	
E_θ	711,000 psi	E	30,000,000 psi
E_r	K_1=1.05	G	11,500,000 psi
	K_2=40.86	ν	0.3
E_z	711,000 psi	R_{outer}	1.9 inch
G_{rz}	337,040 psi		
$\nu_{\theta r}$	0.01		
ν_{zr}	0.01		
$\nu_{\theta z}$	0.3		
t	0.002 inch	**Winder Parameters**	
		T_w	2.0 pli / 2.04 pli

Table 1: Material Properties

The Young's Modulus value of E_θ was tested by performing a stretch test on the 6 inch wide polyester film. This test was performed by Good and Beisel and resulted in an E_θ value of 711,000 psi. Since the test had occurred recently, this value was accepted for this study. The Young's Modulus value of E_z was assumed to be equal to E_θ. The Young's Modulus value of E_r, which is shown in Table 1 as constants K_1 and K_2, was previously tested by Good and Markum [5] and the values reported in Table 1 were accepted for this study since the test had occurred recently.

The Poisson's Ratios were not as easy to obtain. In most cases, for polyester film, values of 0.3 for $\nu_{\theta z}$ and 0.01 for $\nu_{\theta r}$ and ν_{zr} are used. The θz-direction Poisson's Ratio could be approximated in the following way. A strain gage was attached to the centerline of a single sheet of vertically hanging web. Different loads were hung from the sheet of web and MD and CMD strains were recorded. By plotting the absolute value of the CMD strains against the MD strains, a trend line could be produced and a Poisson's Ratio could be inferred from the equation of the trend line. The test was repeated three times and the average value of $\nu_{\theta z}$ was 0.3. To further justify the use of 0.3 for $\nu_{\theta z}$, a few comparison plots were made to compare other values of 0.35 and 0.4 while holding $\nu_{\theta r}$ and ν_{zr} constant at 0.005. Figure 3 shows how the radial stress changes with changing $\nu_{\theta z}$. The change is not great, but there is enough of a change to make a difference when using these values to calculate strains for comparison with the experimental strain values.

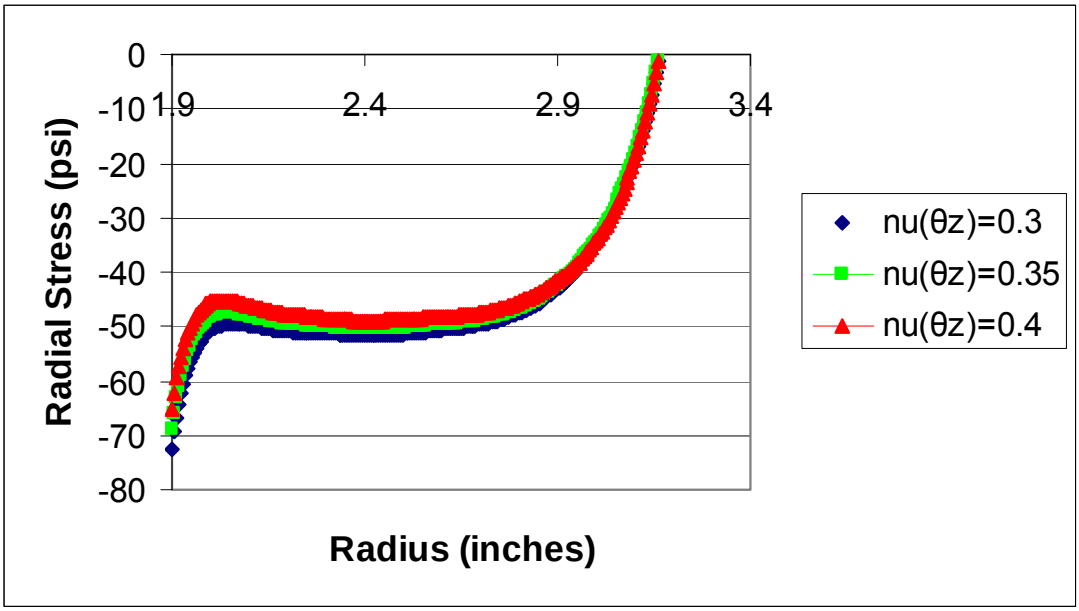

Figure 3: Changing Radial Stress with Changing $\nu_{\theta z}$ and Constant $\nu_{\theta r}$ and ν_{zr}

Figure 4 shows the changing tangential stress with changing $\nu_{\theta z}$. Again, there is not a great change in the values, but any change will affect the calculated strain values.

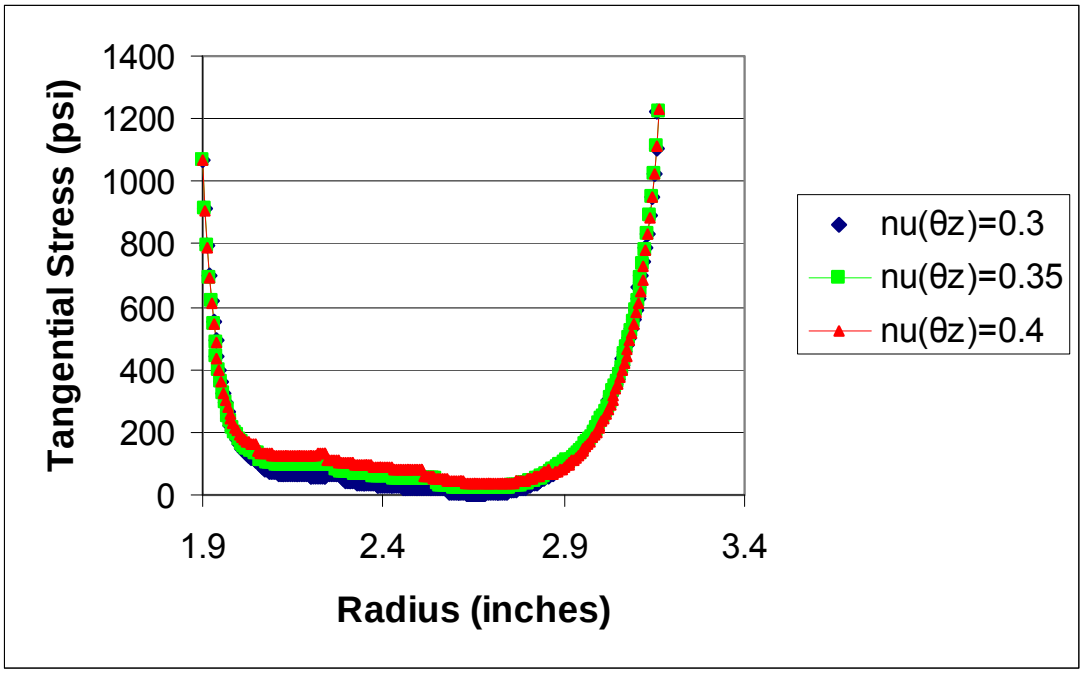

Figure 4: Changing Tangential Stress with Changing $\nu_{\theta z}$ and Constant $\nu_{\theta r}$ and ν_{zr}

Figure 5 shows the changing axial stress with changing $\nu_{\theta z}$. This plot shows a big change in the axial stress as $\nu_{\theta z}$ is changing. The difference is nearly 100 psi in some places which will most definitely change the calculated strain values. After determining from the data that Poisson's Ratio, $\nu_{\theta z,}$ should be 0.3, that value was held constant and Poisson's Ratios $\nu_{\theta r}$ and ν_{zr} were changed to see how the stresses were affected again.

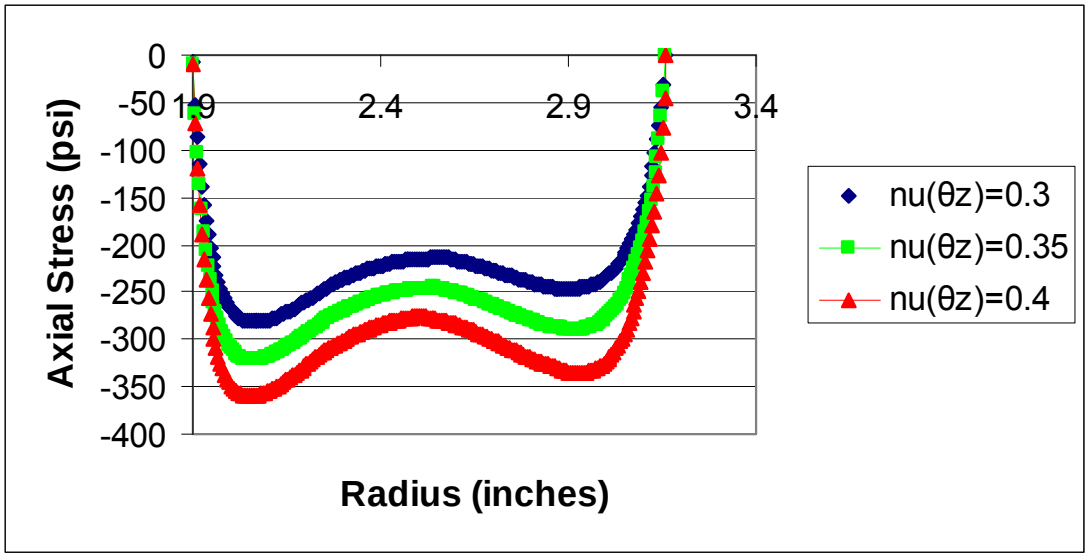

Figure 5: Changing Axial Stress with Changing $\nu_{\theta z}$ and Constant $\nu_{\theta r}$ and ν_{zr}

The θr- and zr-directions could not be approximated in the same way as the θz-direction. A value of 0.01 was measured by Willet and Poesch [10] and accepted for use by Hakiel [1]. This is the value that was used in this study.

Finally, the shear modulus could be calculated by using the Young's Modulus values and the Poisson's Ratios. There were two possible equations for the calculations of the shear modulus. Whether the two expressions are a reasonable approximation is currently unknown because experimental verification does not appear to exist.

The first equation, developed by Szilard [15], is shown below:

$$G_{rz} = \frac{\sqrt{E_\theta \cdot E_z}}{2 \cdot \left(1 + \sqrt{\nu_{zr} \cdot \upsilon_{\theta z}}\right)} \quad , \tag{3.7}$$

and the second equation, derived by Cheng [16], is shown below:

$$G_{rz} = \frac{E_\theta \cdot E_z}{E_\theta \cdot \left(1 + \nu_{\theta z}\right) + E_z \cdot \left(1 + \nu_{zr}\right)} \quad , \tag{3.8}$$

Calculations for both equations were computed and the results were very similar. Equation 3.7 produced a G_{rz} value of 337,040 psi and Equation 3.8 produced a G_{rz} value of 307,792 psi. Since this particular parameter had a minimal effect on the model output, the first value from Equation 3.7 was chosen for input to the axisymmetric code.

The final web material property to find was the thickness of the web. Per the manufacturer, the thickness was reported to be 0.002 in., but this was verified with digital micrometers. The material properties, E, G, and ν, of the steel core were researched from a general materials science text [17].

After input of the information from Table 1 to the axisymmetric code, the theoretical values of stress ($\sigma_r(r,z)$, $\sigma_\theta(r,z)$, and $\sigma_z(r,z)$) for the wound rolls were known. Three different stresses in the wound roll were evaluated against the roll radius: radial stress, tangential stress, and axial stress.

Now that the material properties were known for the web material and the core material, the only thing left to determine for the model were the boundary conditions. The core boundary condition used in the one-dimensional models was also satisfied by this model. The first few layers of quadrilateral elements modeled the core. Core modeling differs in two-dimensional modeling from the one-dimensional modeling, in that two-dimensional models allow any core which can be defined in the axisymmetric plane. Therefore, many more types of core can be modeled, such as cylindrical tubes, cylindrical tubes with one or two end closures, cylindrical tubes supported by an expanding core shaft, or cylindrical tubes supported by an expanding core stub shaft. Cylindrical cores with orthotropic properties in cylindrical coordinates could be modeled and the properties could change with the core radius.

The Lagrangian constraint method was used to establish the outer boundary condition of the winding tension across the width of the web. The method assumed that the layers of the web, in the form of cylinders, would be accreted to the outside of the winding roll. The cylinder would have a relaxed radius, before becoming the outside layer on the winding roll. The relaxed radius could change and the cylinder would then become a generic axisymmetric shape across the width of the web. This axisymmetric shape could accommodate both the length and thickness non-uniformity across the web width. In this case, this was no major length or thickness non-uniformity. The two-dimensional model would allow the study of stresses that were nearly plane stress at the roll edges versus the roll interior, which may approach plane strain conditions if the roll was wide enough. The Lagrangian constraint of the following form was enforced over several nodal points across the width of the winding web:

$$u_j - u_i = \delta_{ij} \quad , \tag{3.9}$$

where δ_{ij} was the level of interference between the cylinder and the outside of the previous layer which was last added to the wound roll. This relative constraint forced the outer layer cylinder outward and the outside of the layer beneath inward until the two surfaces come together to some radial position. The circumferential stresses, σ_θ, were computed and averaged across the width of the web.

The enforcement of the outer boundary condition was an iterative solution and only stopped when the average circumferential stress and the average web line tension became equal. The computation for this process was not difficult since several thousand layers compose a wound roll and the relaxation radius described for adding the last lap was a good starting assumption for the relaxation radius of the next lap that was added.

Model Outputs

Now that all the parameters needed for running the axisymmetric code were known and understood, the winding model was examined in two ways. First, three-dimensional plots will be presented to show how each of the three stresses change as a function of radius of the wound roll and segment of width being analyzed. These plots will demonstrate how σ_r, σ_θ, and σ_z vary as a function of radius and axial location in the wound roll. The three-dimensional analysis will be done for both the 6 inch material and the 24 inch material.

Second, two-dimensional plots will be presented to show how each of the three stresses change as a function of radius only. In these series of plots, the stress data will be taken from segment 3, which represents the centerline of the wound roll. The 6 inch material stresses will be plotted with the 24 inch material stresses so that a comparison of the two widths can be made. These plots will later be used to compare with the experimental results where strain data was taken at the centerline of the wound roll.

The first set of plots that are discussed are the three-dimensional plots for the 6 inch wide material. Figure 6 shows the plot of the radial stress, σ_r, as a function of the wound roll radius and the width segment. The radial pressure is simply the negative of the radial stress, so the greatest radial stress will be seen near the core where the radial pressure is the greatest. The edges of the roll's width at the core see greater radial stresses than the center of the roll's width at the core because of the plane strain condition. The axial stresses are near zero at the core and this affects the radial stresses at the core as well. The radial stress is near zero at the outside of the wound roll because of surface equilibrium in the radial direction.

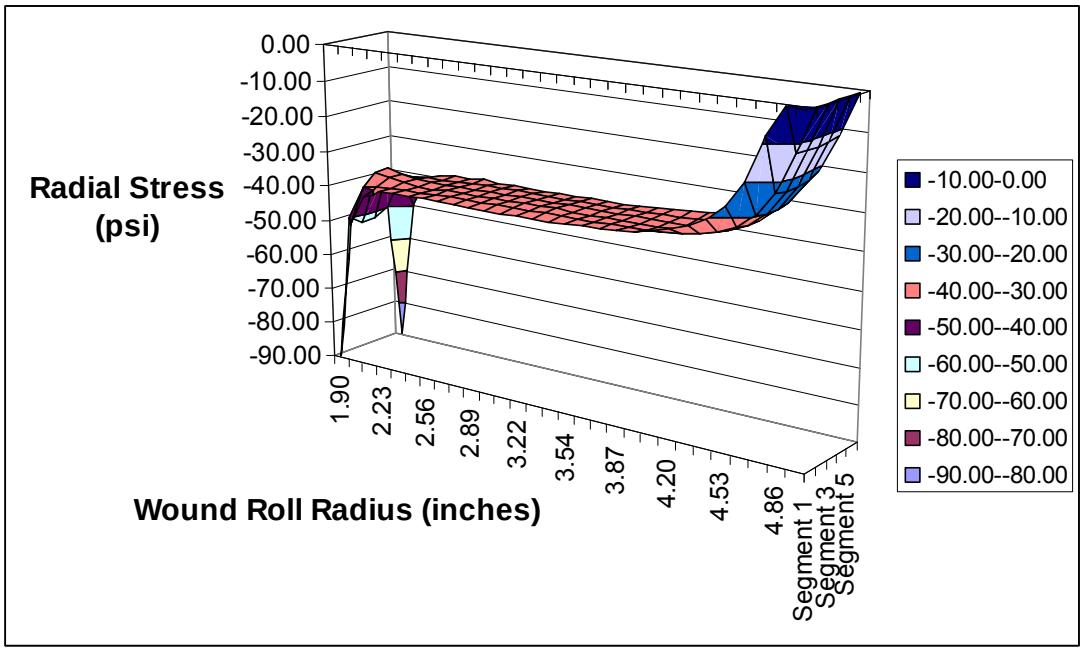

Figure 6: Radial Stress Through 6 inch Web

Figure 7 shows the plot of the tangential stress, σ_θ, as a function of the wound roll radius and the width segment. The tangential stress starts off quite high and then goes to nearly zero. The outside edges of the roll's width in the winding roll dip even lower than the center part of the roll's width in the winding roll. Lower tangential stresses are seen within the winding roll because radial compression causes the decrease within the roll. The edges see even lower tangential stresses because of the plane strain condition. The general equation for the tangential stress is the winding tension divided by the web thickness, which gives a tangential stress of 1000 psi. This is the stress that should be seen at the core and at the outside of the wound roll. As seen in Figure 7, The outside of the wound roll is nearly 1000 psi, but the core's tangential stress is slightly less than 1000 psi and closer to 900 psi. This is because the axisymmetric code that was used makes the average tangential stress of the inside and outside roll radius equal to the 1000 psi.

Therefore, there will be some segments at the inside or outside roll radius that have tangential stresses less than or greater than 1000 psi.

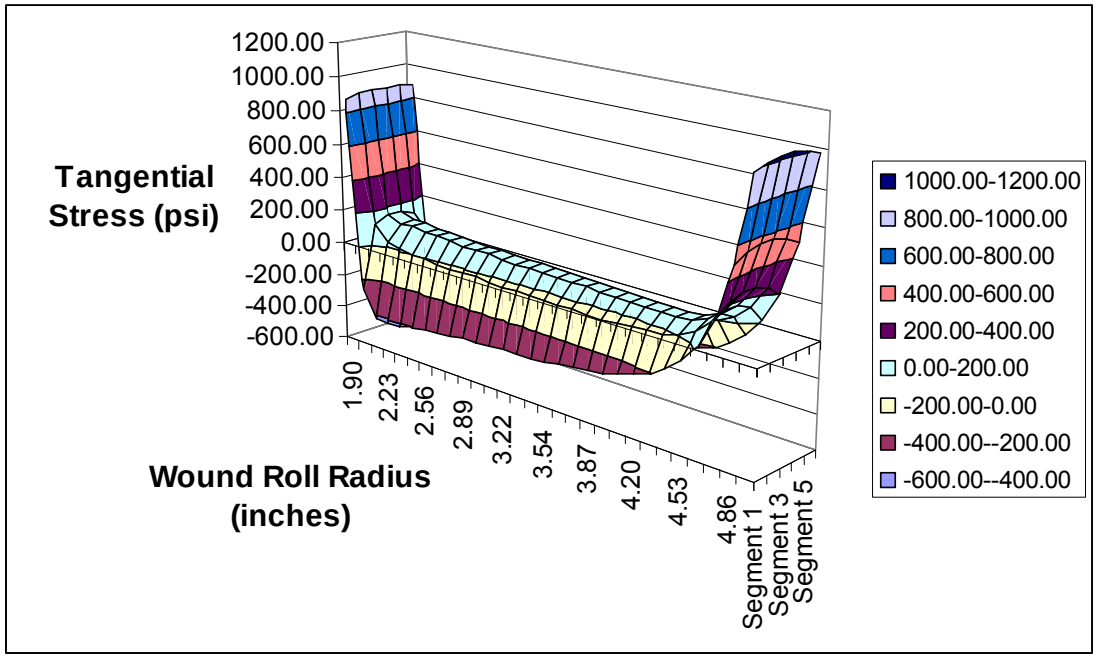

Figure 7: Tangential Stress Through 6 inch Web

Figure 8 shows the plot of axial stress, σ_z, as a function of wound roll radius and width segment. At radii values close to the core, the core and web materials are being modeled as though they are stuck together and trying to deform as one, but they are two different materials with two very different Young's Modulus values. The core's modulus is moving laterally in a different way than the web, so there is a sharp dip in axial stress where the two are modeled together until the web separates and starts being modeled on its own. Then, the axial stress approaches zero because it is close to plane stress conditions.

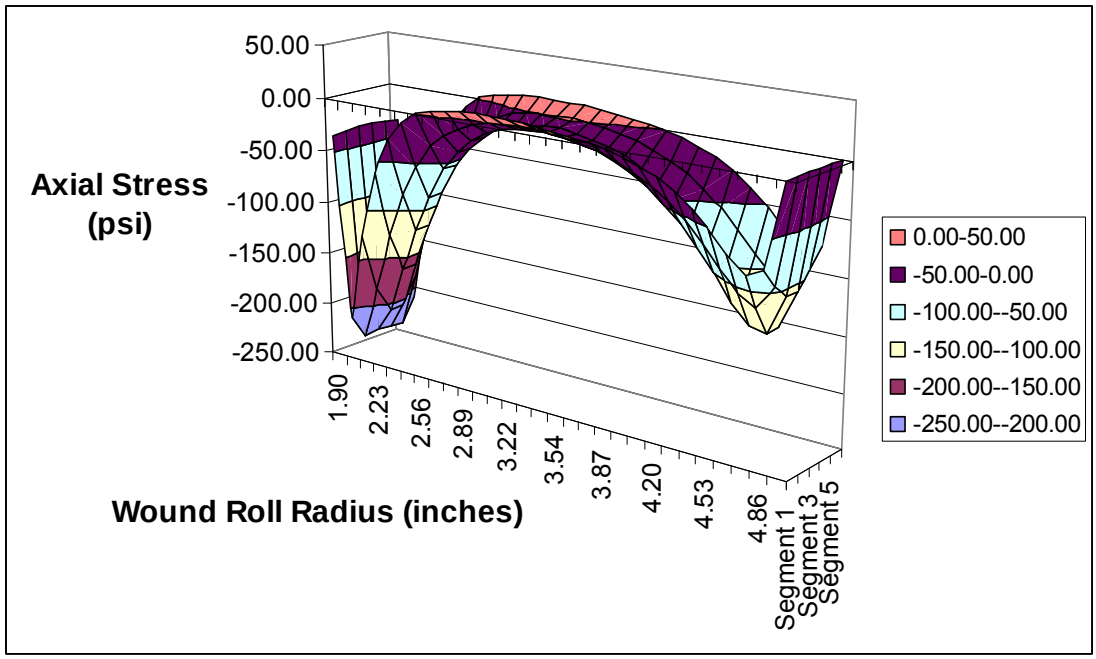

Figure 8: Axial Stress Through 6 inch Web

The next set of plots that are discussed are the three-dimensional plots for the 24 inch wide material. Figure 9 shows the radial stress, σ_r, as a function of the wound roll radius and the width segment. Just as with the 6 inch wide material, the 24 inch wide material shows the greatest radial stress at the core where the radial pressure is the greatest. While the edges of the roll's width at the core saw the greatest radial stress, the difference between the edges of the roll's width and the center of the roll's width at the core were not as great as with the 6 inch wide material. Again, the outside of the roll's wound radius shows a radial stress of nearly zero because of surface equilibrium in the radial direction.

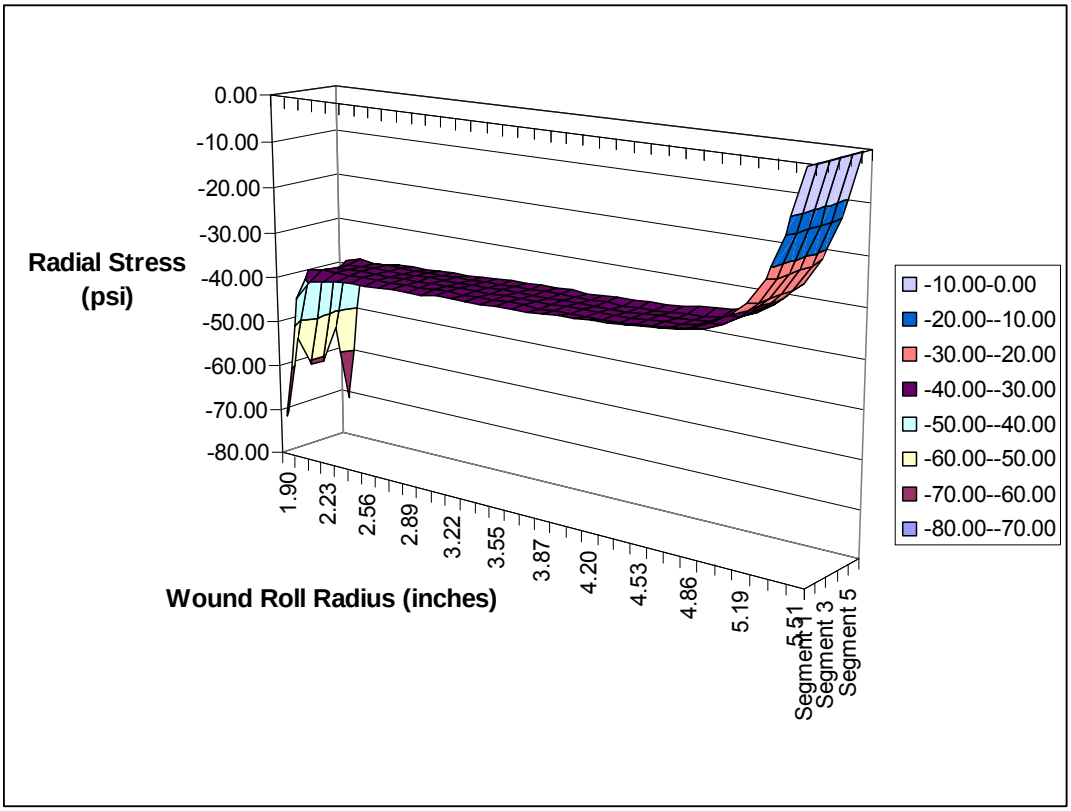

Figure 9: Radial Stress Through 24 inch Web

Figure 11 shows the tangential stress, σ_θ, as a function of the wound roll radius and width segment. The greatest tangential stresses are seen at the core and at the outside roll radius. The calculated tangential stress was slightly higher than for the 6 inch wide web. This was because when web width was entered into the HSWL, a width of 24.5 inches was entered instead of 24 inches. The web tension of 2 pli was converted by multiplying it by 24.5 inches and then dividing that answer by 24 inches. The resulting web tension was 2.04 pli for the 24 inch wide web. The calculated tangential stress for the outside roll radius was 1020 psi. When taking an average of the outside roll radius tangential stress, the average was 1005 psi. The segment within the winding roll saw nearly zero tangential stress, while the edges of the width of the winding roll saw even less tangential stress. The difference between the edge tangential stress and the center

tangential stress of the winding roll was not as great as with the 6 inch wide material. This was once again because the 24 inch wide material was not in a plane strain condition.

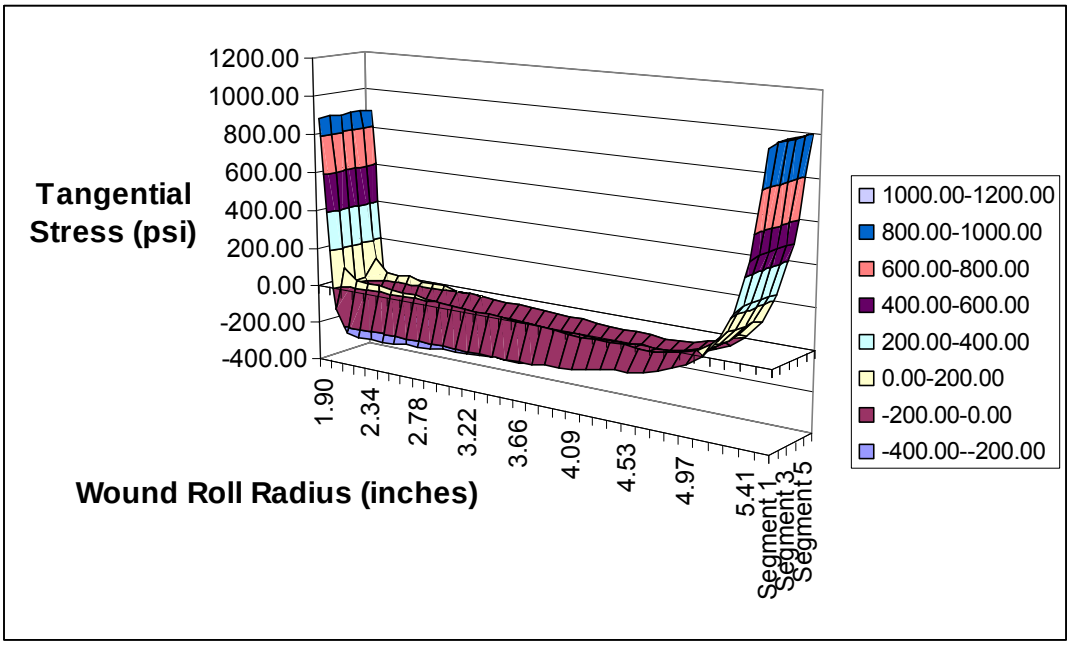

Figure 10: Tangential Stress Through 24 inch Web

Figure shows the axial stress, σ_z, as a function of the wound roll radius and the width segment. The axial stresses in the 24 inch wide web have a different trend than in the 6 inch wide web. The first difference is that the web and core do not appear to be 'stuck together' as they were in the 6 inch material. The axial stresses are the greatest at the core, but then fall to greater negative values within the winding roll. The edges of the roll's width within the winding roll have a higher axial stress, but still not near zero. The outside radius of the wound roll show axial stresses of near zero. As seen from Figure, the 24 inch wide web is not in plane stress or in plane strain, but is somewhere in between the two.

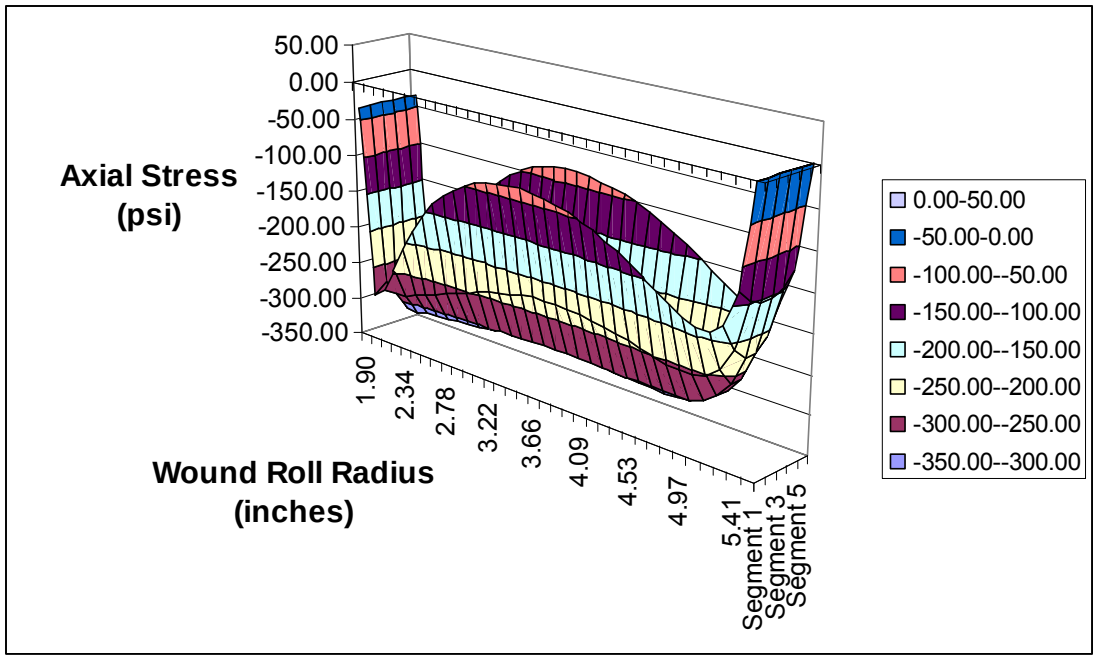

Figure 11: Axial Stress Through 24 inch Web

In the next group of plots, the three stresses were plotted as a function of radius only. The median data for both the 6 inch wide web and the 24 inch wide web were plotted together so that comparisons between the two widths could be made. The median data was the data set for segment 3 for both widths, which represented the centerline of the roll's width.

The first comparison, shown in Figure , shows the changing radial stress with changing wound roll radius. As previously stated, the radial stress is simply the negative of the radial pressure, so the greatest radial stress occurs at the core where the radial pressure is the greatest. With both the 6 inch wide web and the 24 inch wide web the radial stress goes to zero at the outside of the wound roll because of the surface equilibrium in the radial direction. The 6 inch wide web saw less radial stress at the core than the 24 inch wide web because the final wound radius was less than the 24 inch wide web.

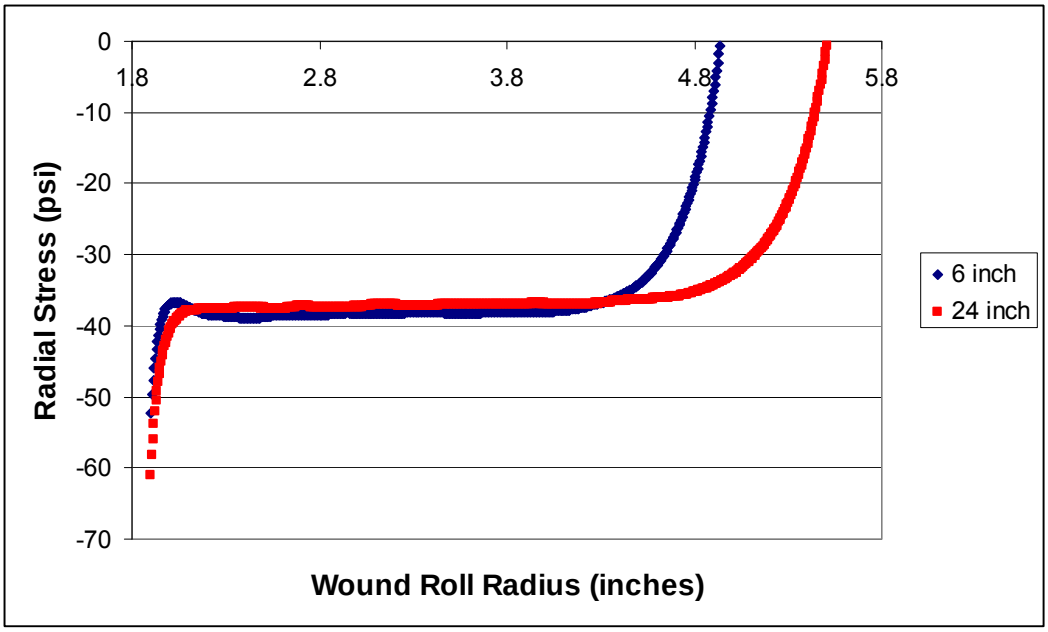

Figure 12: Radial Stress in Wound Roll of PET

The next comparison, shown in Figure , shows the changing tangential stress with changing wound roll radius. As the two different widths of material show, the greatest tangential stress occurs at the core and at the final wound roll radius. The tangential stress of the outside wound roll radius is higher than the tangential stress at the core because of the averaging method used by the axisymmetric code described earlier in this chapter. This value was 1000 psi for the 6 inch wide web and 1020 psi for the 24 inch wide web. Segments 3 and 4 had the highest values for the tangential stress in the average.

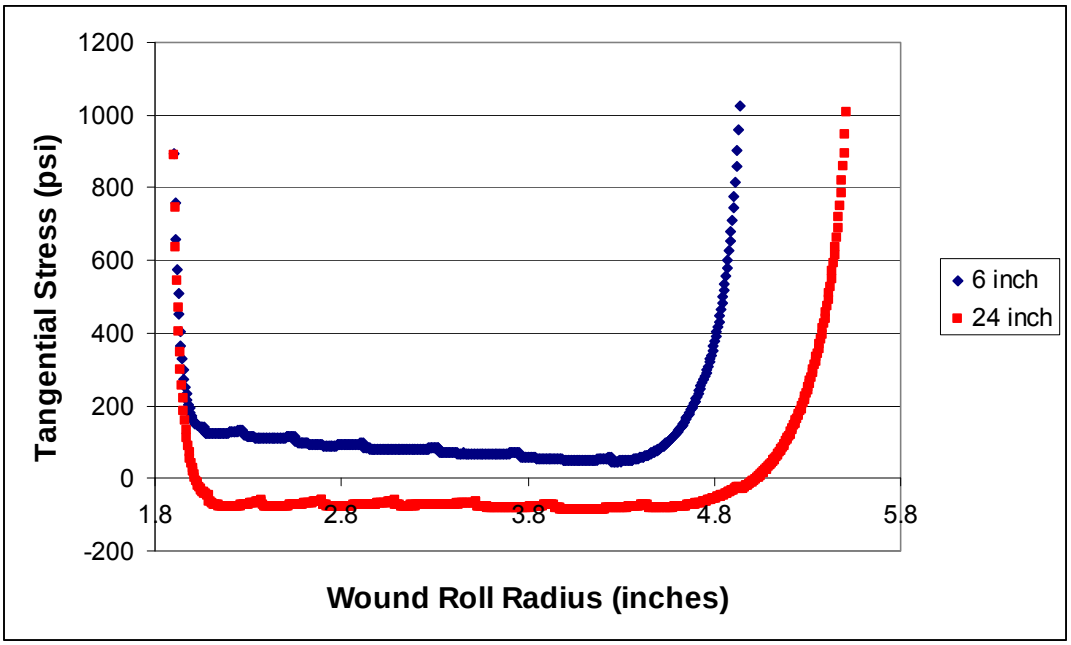

Figure 13: Tangential Stress in Wound Roll of PET

The final comparison is shown in Figure . The changing axial stress for the two widths is shown with the changing wound roll radius. As previously discussed in the three-dimensional analysis, the 6 inch wide web was approaching plane stress conditions and the 24 inch wide web was not in plane stress or plane strain, but was somewhere in between. This is seen again in Figure for the median data plots. While both widths of web have axial stresses of zero at the final wound roll radius, the similarities end there. The 6 inch wide web starts at nearly zero axial stress and the core and web are modeled together, but deforming at different rates for a short time. The web is then modeled alone and approaches plane stress conditions. The 24 inch wide web also starts with an axial stress of nearly zero and then falls to a negative value of about -300 psi before coming back up to zero at the final wound roll radius. The 24 inch wide web is between plane stress and plane strain conditions.

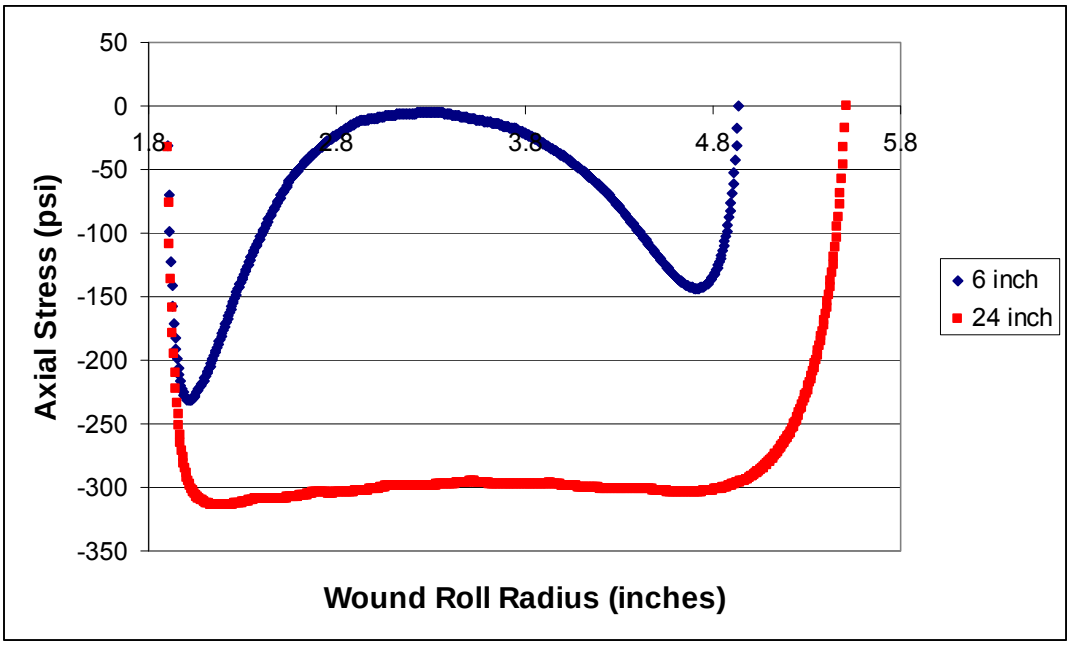

Figure 14: Axial Stress in Wound Roll of PET

The stresses that were described in this chapter were a good approximation for what was expected during the experimental portion of this study. These stresses will later be converted to strains and compared to the experimental results for further analysis.

CHAPTER IV

EXPERIMENTAL PROCEDURE

In order to measure the strain within the wound roll, the use of several strain gages were required. Two different types of strain gages were used: a single element strain gage and a rosette strain gage. The two different types of gages were used to see if strains obtained experimentally differed because of the type of gage used. Each was attached to the web in such a way to measure both MD strains and CMD strains.

The rosette gage was a Micro-Measurement Precision Strain Gage (type CEA-13-250UT-350). The gage had 350 ohms of resistance and a nominal gage factor of 2.10 +/- 1.5%. The rosette gage was actually two single element gages on a single backing that were turned 90º to one another, so that one measured CMD strain and the other measured MD strain. Figure 11 shows an example of a rosette strain gage.

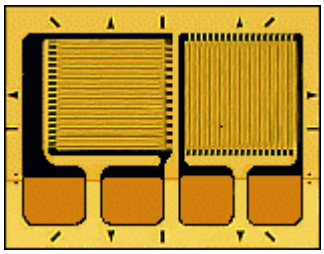

Figure 11: Rosette Strain Gage

The single element gage was a Vishay Micro-Measurement Student Gage (type CEA-13-240UZ-120). The gage had 120 ohms of resistance and a gage factor of 2.10 +/- 0.5%. Two single element gages were used 90º apart from one another, so that CMD and MD strains could be measured just as the rosette gage did. The two gages were attached 180º apart from one another on the wound roll so as not to create too much disturbance in the winding in one location. Figure 12 shows an example of a single element strain gage.

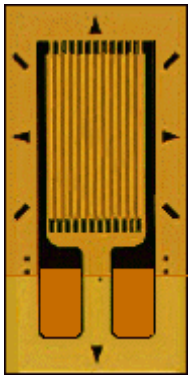

Figure 12: Single Element Strain Gage

The method of attachment of the strain gage to the web was the same for each type of strain gage. First, the web surface was roughed slightly using very fine grit sandpaper. The purpose of this procedure was to make the surface less slick so that the adhesive that was placed on the strain gage had a rougher surface on which to adhere on the web surface, therefore making a better connection to the web surface. The strain gage was then attached to the web using a cyanoacrylate, or M-Bond, adhesive. Figure 13 shows an example of the completion of the strain gage attachment.

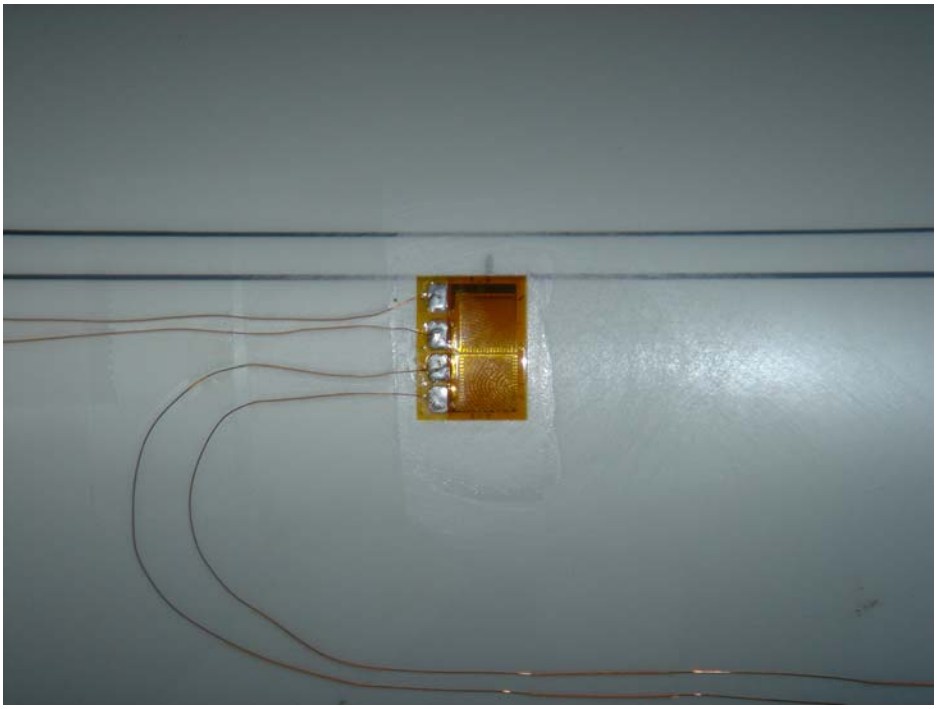

Figure 13: Strain Gage Attachment

Thin copper wires of 0.0063 inch in diameter were soldered to the strain gages. At the end of each copper wire, a larger piece of 12 gauge copper was attached by soldering the two pieces of wire together. This served as a stronger piece to insert into the wide-range strain indicator, which was used to measure the strain in the wound roll. The thin copper wire was easily broken when attached and detached from the strain indicator repeatedly. During preliminary testing, when using the larger piece of copper wire to insert in and out of the strain indicator, the wires would remain unbroken and measurements could retain consistency because the length of wire used was not diminished. The change in resistance of a strain gage is small due to a change in strain. Thus, it was important that any change in resistance in the gage-lead system not associated with strain be minimized.

As previously mentioned, the wide-range strain indicator was used to take measurements of strain from the wound roll. These measurements were reported in units of micro-strain from the strain indicator. Figure 14 shows a picture of the wide-range strain indicator used in the experimental portion of the study.

Figure 14: Wide-Range Strain Indicator (Model 3800)

After the gages were attached to the web and wired appropriately, a web tension of approximately 2 pli (pounds per linear inch of web width) was applied to the web. The tension was held in the web even while the web was not moving. This gave the opportunity to take the strain measurement accurately. The first strain measurement collected from the strain indicator was at the point where the strain gage was attached. The strain gage was attached on the surface of the wound roll along the centerline of the width of the roll. The gage was mounted on the outside surface of the wound roll, as

shown in Figure 15. The gage was mounted on the curved part of the roll and not in the free span.

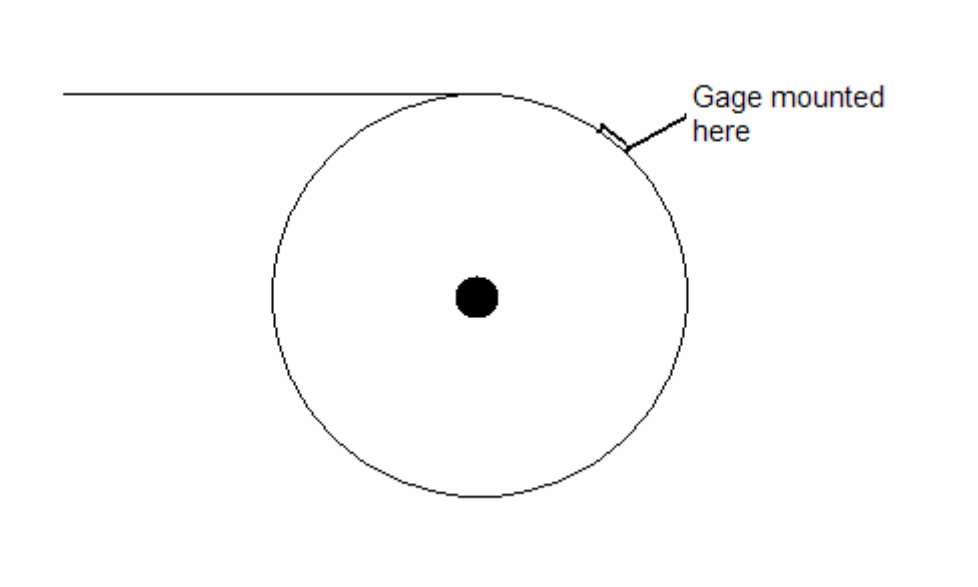

Figure 15: Placement of Strain Gage on Wound Roll

At this point, the reading on the indicator was balanced to read zero. This meant that all bending strain involved in the wound roll and all membrane strain associated with the 2 pli web tension was now balanced out, or nulled, with the strain indicator.

Subsequent strain measurements were collected using the strain indicator. The web was allowed to wind at a speed of 50 ft. per minute and the 2.0 pli web tension was maintained. Strain readings were taken at 5 minute intervals. At the 5 minute mark, the machine was changed from 50 ft. per minute to 0 ft. per minute so that the strain measurement could be taken while the web was holding steady, but still had the required web tension applied. Figure 16 shows an example of taking a strain measurement with the strain indicator.

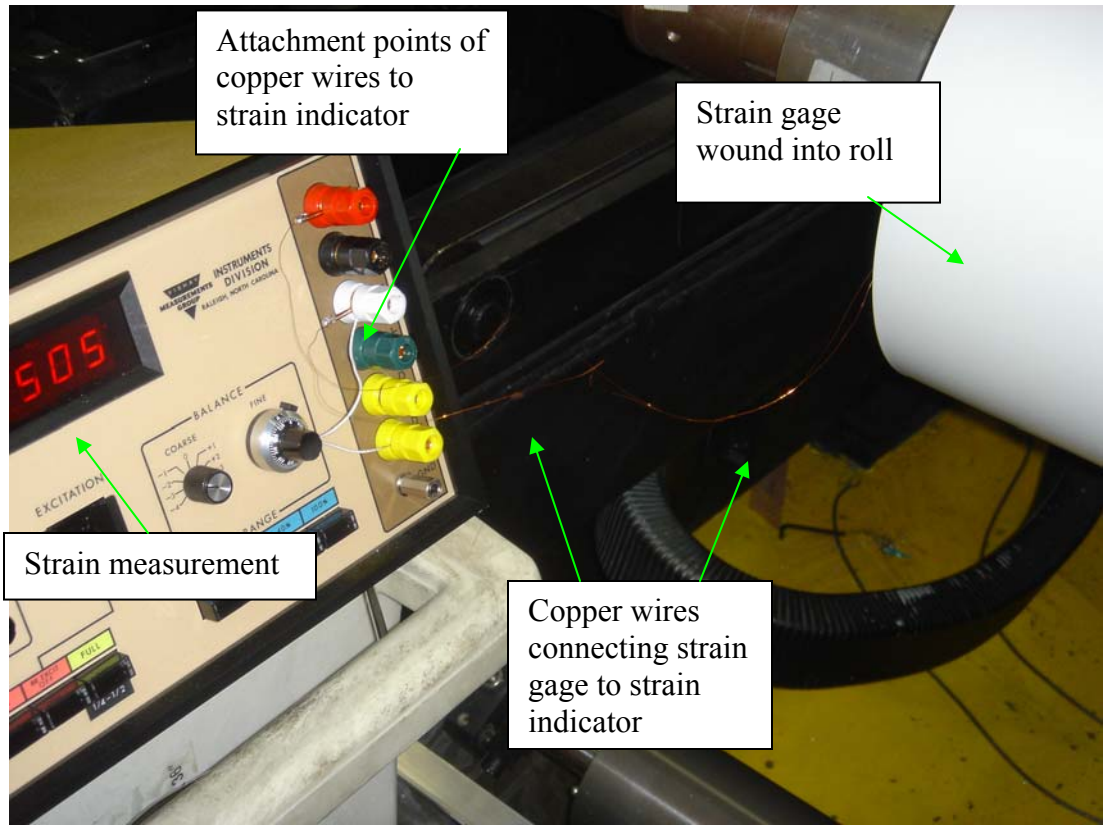

Figure 16: Collection of Experimental Strain Data

At each strain reading, the pile height of the roll was also recorded using a set of calipers. The pile height of the roll was measured from the surface of the core to the surface of the wound roll. A demonstration of this is shown in Figure 17.

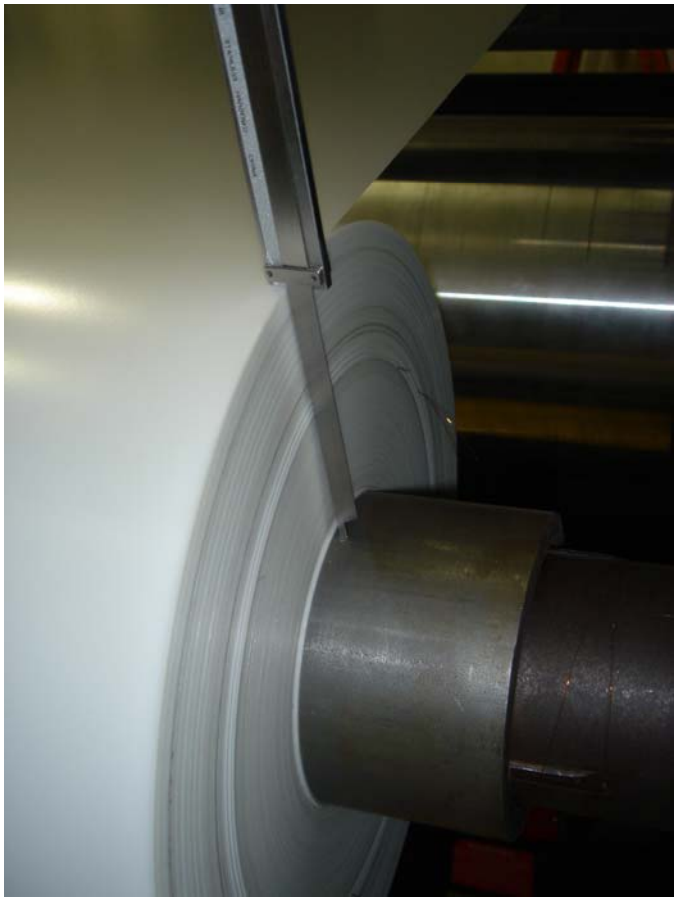

Figure 17: Measurement of Pile Height

This process would continue for the next 5 to 7 strain readings, at which time the strain value would have become constant and the experiment would be over. At each reading, the wires were connected to the strain indicator to take a strain reading and then disconnected in order to wind the roll.

Before the actual experimental data could be collected, there were a few factors that needed to be addressed. The first concern regarded using the strain gages on the web and whether this supplied any kind of reinforcement factor to the web material, thus changing the strain measurement in some way. The next concern was the validity of the data taken when the wires were disconnected for winding the roll and reconnected to

measure the strain. A simple set of tests was devised that addressed both of these concerns.

The first of the two tests was done on a single sheet of web material. Both types of strain gage were attached to the single sheet of the web, which was approximately 6 feet long and 6 inch wide. The sheet was attached to a height of approximately 10 feet to a firm structure and allowed to hang freely. At the end of the length of web, several different loads were attached and strain readings were taken at the different load intervals. The test was accomplished in two ways. First, the connecting wires were left in the strain indicator continuously as loads were changed and strain readings were taken at each load level. Next, the connecting wires were disconnected at each load level and then reconnected to the strain indicator in order to take a strain reading to simulate the winding conditions. When evaluating the two different ways of taking data against one another, the validity of taking strain data while disconnecting and reconnecting the wires at each reading interval could be determined. When evaluating the strain reading against the theoretical strain calculated for the length of freely hanging web, the reinforcement factor could be determined. The reinforcement factor calculation was:

$$\frac{\varepsilon_{theoretical}}{\varepsilon_{experimental}} = \alpha \quad , \tag{4.1}$$

where α was the reinforcement factor coefficient. The theoretical strain was found using the following equation:

$$\varepsilon_{theoretical} = \frac{\frac{P}{t \cdot w}}{E} \cdot 10^6 \quad , \tag{4.2}$$

where P is the load applied to the web, t and w are thickness and width of web respectively, and E is the Young's modulus of the material. The entire equation is multiplied by 10^6 to give units of μS.

Since the actual experiment would not be taking place on a single sheet of free hanging web, but on a wound roll of web, a second reinforcement factor test was conducted. This test was done on a small roll of wound web, 6 inches wide and with 2.001 inches of pile height, which gave a final radius of 3.901 inches. The strain gage was mounted at a pile height of 1.01 inches, or at a radius of 2.91 inches. The roll was placed on the side in an Instron 8500 Material Testing Machine and different axial loads were placed on the roll while strain readings were taken. These readings were then compared to the theoretical strains that would be placed on such a roll and the reinforcement factor was determined. The theoretical strain was found using the following equation:

$$\varepsilon_{theoretical} = \frac{\frac{P}{\frac{\pi}{4}\cdot\left(d_o^{\,2}-d_i^{\,2}\right)}}{E}\cdot 10^6 \quad , \tag{4.3}$$

where P is the load applied by the Instron machine to the wound roll in the axial direction, d_o is the final diameter of the roll, d_i is the diameter of the core ,and E is Young's modulus. The two diameter values were used because the test fixture compressed all material outboard of the core. Again, the equation was put in units of μS by multiplying the equation by 10^6.

As previously described, strain data was read in two different ways from the strain indicator. The first set of data was taken while the copper wires were constantly connected to the strain indicator and the loads were placed on the web. The next set of

data was taken with the copper wires disconnected at every load interval and re-connected for the strain reading. The continuously connected case was repeated three times and the disconnected case was also repeated three times. The two types of test were compared to one another, with the continuously connected case being the reference test. The results of the continuously connected versus disconnected tests concluded that there was a 4% to 12% difference and a 1% to 12% error in the two methods of taking strain data. This was deemed acceptable, considering the extreme difficulties in leaving the copper wires attached during the winding portion of the test cases.

The next pre-experimental test was just as important, but dealt with how to interpret the strain data once it was collected in the winding tests. The first reinforcement factor test was performed on a single sheet of web material hung vertically with various loads applied. At this point, all the data taken was acquired as if performing the actual experiment, i.e. disconnecting the copper wires between each reading. The test evaluated strains in the machine direction, since that was how the load was being applied. The resulting reinforcement factor, calculated using Equation 4.1, ranged from 2.15 to 2.37.

The final pre-experiment test was another reinforcement factor test, but for the axially applied load. The resulting reinforcement factor ranged from 0.99 to 1.19. This concluded that when winding the roll, as in the actual experiment, there was no significant reinforcement factor involved for collecting strain readings. Thus, once the web with a strain gage attached was wound into a roll composed of hundreds or thousands of other layers it appeared the reinforcement factor was near unity. This meant that the strain indicated by the strain indicator did not have to be corrected for reinforcement effects during the winding tests.

With the experimental procedure and preliminary tests complete, the results could be calculated. The next two chapters deal with the results of the experimental data and the comparison of these results with the results from the two-dimensional model.

CHAPTER V

EXPERIMENTAL RESULTS

The results of the experimental data can now be introduced. It should be noted that a total of 20 tests were performed, but only 9 test results will be shown. The other 11 tests reported bad data because of various user errors including: taking erroneous strain readings by improper balancing, not attaching gages properly, and copper wires breaking at the roll's edge during strain testing. The user errors were obvious during testing and the results of those tests were eliminated from the study. All test results are shown in the Appendix.

As previously stated, two different roll widths were tested, 6 inch and 24 inch wide webs. The same rolls of each width were used for each test repeat, but new strain gages were applied for each new test. While two different strain gages were used in testing, the differences in the results were insignificant. The two gages were of different sizes but produced similar results. This reinforced the finding that the reinforcement factor was near unity after the gage had been wound into the roll.

The following plots show the two different strains that were obtained in the experiment versus the radial depth of the strain gage in the wound roll. The radial depth of the strain gage into the wound roll was determined by subtracting the radius at which the gage was attached from the radius at which the strain reading was taken. The first tests evaluated were at a roll width of 6 inches. In Figure 18, five of the fourteen tests for the 6 inch wide material were evaluated. The MD strains were evaluated first. As seen in Figure 18, the repeatability for MD strain readings was quite good.

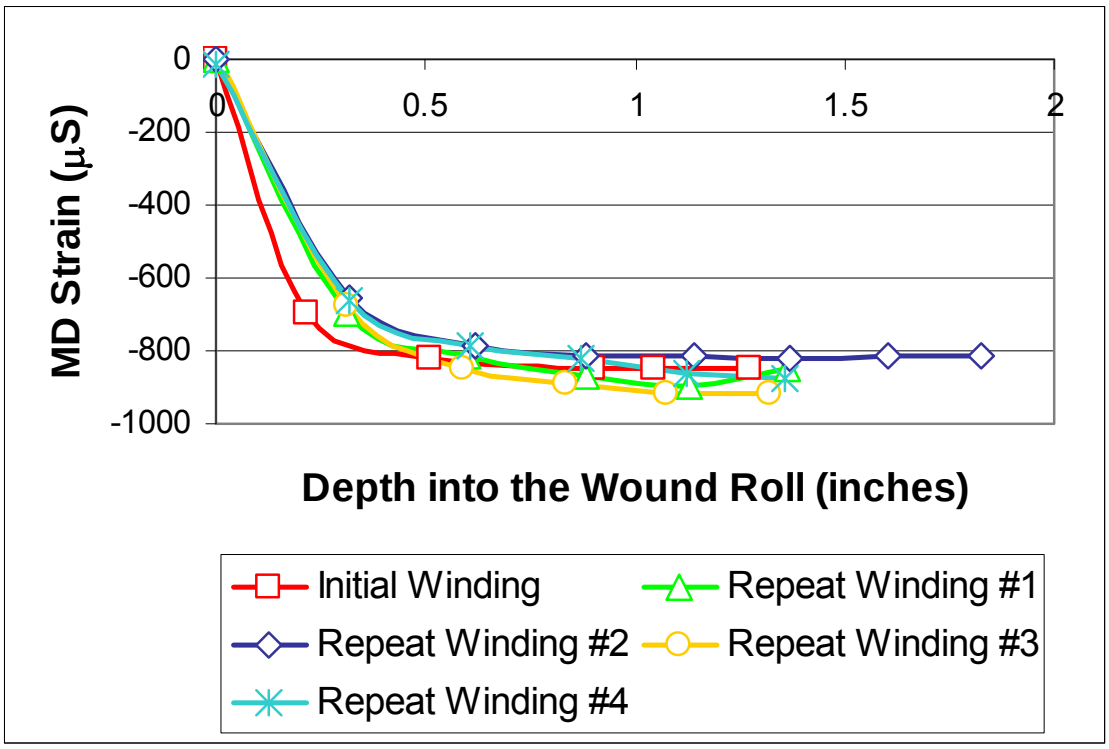

Figure 18: MD Strains in 6 inch Wide PET

Statistical interpretation was taken at three different points in the depth of the strain gage in the wound roll. Those results are shown in Table 2. The repeatability for this set of data was very good, which is seen in Figure 18 and in Table 2. One important values to look at in Table 2 is the standard deviation. The standard deviation represents the average distance of the measured strains from the mean strain value. This value is on

the low side, showing that all of the strain data taken was fairly close together. This particular set of tests was the most repeatable in the study.

0.3		*0.87*		*1.33*	
Mean	-676.6	Mean	-848.2	Mean	-862
Median	-676	Median	-846	Median	-848
Standard Deviation	18.81	Standard Deviation	33.29	Standard Deviation	38.56
Range	40	Range	79	Range	102
Minimum	-696	Minimum	-892	Minimum	-920
Maximum	-656	Maximum	-813	Maximum	-818
Count	5	Count	5	Count	5

Table 2: Statistical Results for MD Strains in 6 inch Wide PET

Figure 23 shows CMD strains for the 6 inch wide web. The CMD strains were only evaluated at the centerline of the web where the strain was the highest. In general, CMD strains were much less repeatable than the MD strains. The range of CMD strain was much greater than the MD strain. The range of the CMD strain was from about 125 μS to 360 μS at a depth of 0.5 inches.

One possible reason for the difference in repeatability between the MD strains and the CMD strains could be that CMD strains were more sensitive to friction. During the winding process, a great deal of static electricity was produced by the roll as layers were wound on. The static electricity produced at least some friction in the layers of the wound roll. This is only one plausible explanation of the decline in repeatability for the CMD strain.

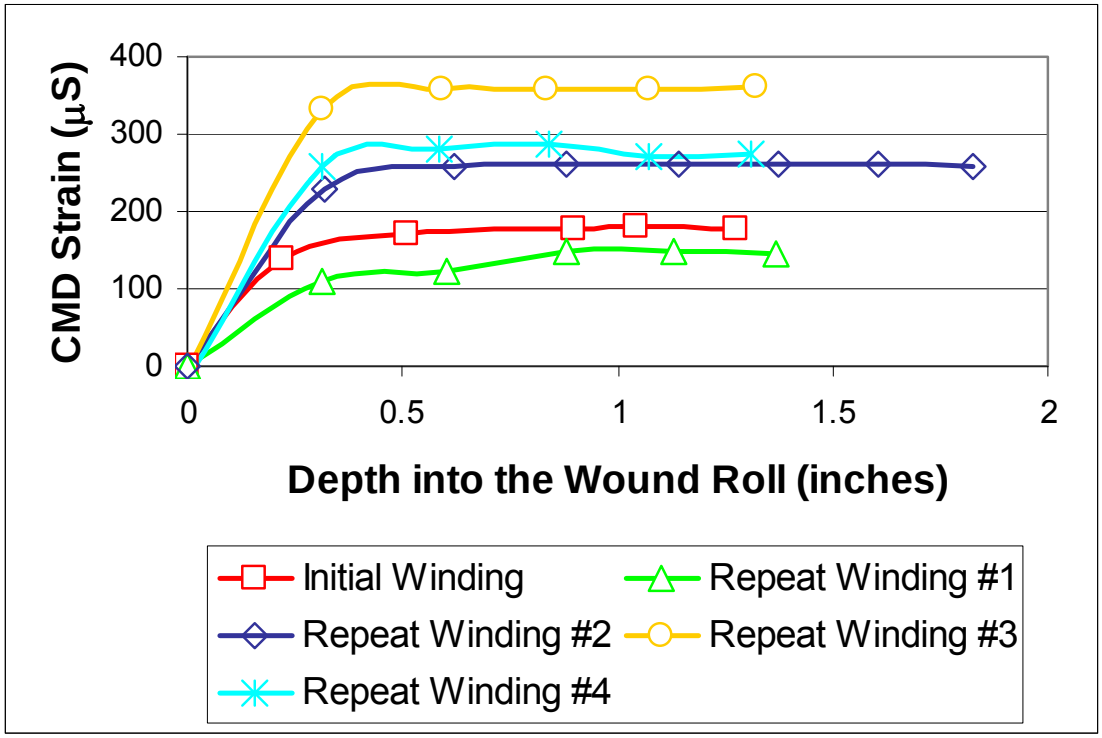

Figure 19: CMD Strains in 6 inch Wide PET

The statistical interpretation is shown in Table 3. Again, by looking at the standard deviation it is obvious that this set of data is not as accurate as the MD data. With the data shown in the plot in Figure 23, the statistical data should not be expected to be as good as the MD statistical data. The repeatability is obviously not as good and therefore the standard deviation and standard error are going to be much higher.

0.3		*0.75*		*1.25*	
Mean	263	Mean	302	Mean	303
Median	228	Median	261	Median	260
Standard Deviation	162	Standard Deviation	169	Standard Deviation	171
Range	399	Range	421	Range	426
Minimum	109	Minimum	147	Minimum	145
Maximum	508	Maximum	568	Maximum	571
Count	5	Count	5	Count	5

Table 3: Statistical Results for CMD Strains in 6 inch Wide PET

The next set of data evaluated were the MD strains for the 24 inch wide material. In this set of data, four of the six tests were used for analysis. The remaining two tests were invalid because of user error as described earlier in this chapter. In Figure 20, the plot of MD strains versus depth of gage in the wound roll is shown. The repeatability for the MD strain was not as good as for the 6 inch wide roll.

In this case, the cause for the decline in repeatability is because of difficulties with the MD strain gage in Repeat Winding #1. This is a good example of an invalid test due to faulty soldering of the copper wires to the strain gage. This, unfortunately, was often not discovered until the test was over and the material was unwound. While the general curve of this particular test was correct, the values were much lower than the other tests. At completion of the test, it was discovered that one of the copper wires had come partially loose from the strain gage. It was unknown at what point in the test this had happened, but since the general curve of the data is correct and only the values appear to be wrong, it would appear as if the wire was loose during the entire test. If Repeat Winding #1 were to be discounted from the MD tests, the data would become much more repeatable. However, it will be seen during examination of the CMD strains that the CMD strain gage of that particular test was soldered correctly and had very good results. Repeat Winding #1 remains in the data set because the cross machine direction strains were much more acceptable.

Since the test directly before and directly after Repeat Winding #1 were basically on top of one another, repeatability is acceptable for this test. Not including Repeat Winding #1, the range of the MD strains was less than 100 μS, ranging from about -430

µS to -500 µS, which is a fairly repeatable range of data, since the MD strains in the 6 inch material varied by about the same amount, ranging from about -800 µS to -900 µS.

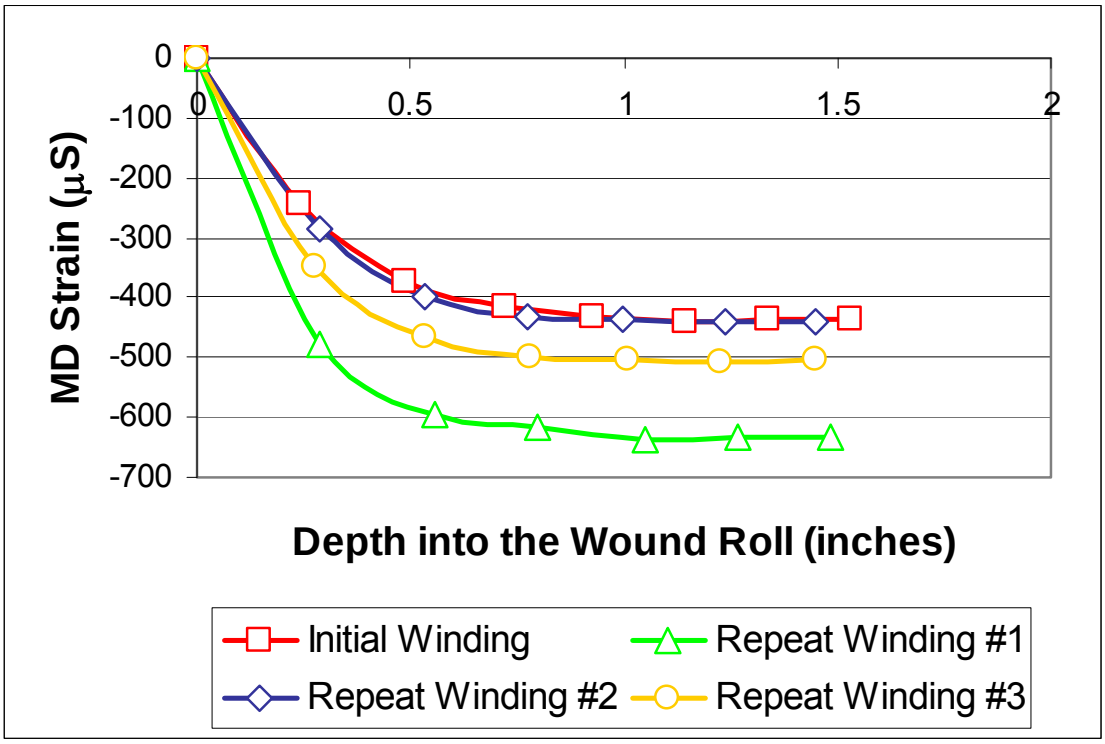

Figure 20: MD Strains in 24 inch Wide PET

As shown in the statistical data in Table 4, the standard deviations for the three depths evaluated were much higher than in the MD strains of the 6 inch wide material. This is only because of Repeat Winding #1. Without that data included, standard deviation would become much lower, as would standard error, making the data set closer to one another and just as good as MD data for the 6 inch wide material.

0.25		0.75		1.5	
Mean	-338	Mean	-490	Mean	-361
Median	-317	Median	-464	Median	-439
Standard Deviation	102	Standard Deviation	91	Standard Deviation	201
Range	234	Range	200	Range	440
Minimum	-476	Minimum	-617	Minimum	-503
Maximum	-242	Maximum	-417	Maximum	-63
Count	4	Count	4	Count	4

Table 4: Statistical Results for MD Strains in 24 inch Wide PET

The CMD strain data for the 24 inch wide material is shown in Figure 21. The four tests that were evaluated produced less than repeatable results. As previously stated, one plausible explanation could be the CMD strain sensitivity to friction. The difference in range was shown in Figure 19 for the 6 inch wide material and if the static electricity explanation holds, the range may be greater in the 24 inch wide material. While there was considerable amounts of static electricity produced when winding the 6 inch wide web, there was even more produced by the 24 inch wide web. This could have produced more friction as well. By examining the plot in Figure 21, the range of CMD strain is from about 100 μS to 500 μS, nearly twice the range of the 6 inch wide material. While this may or may not be the only explanation for the CMD strain, it is certainly still plausible.

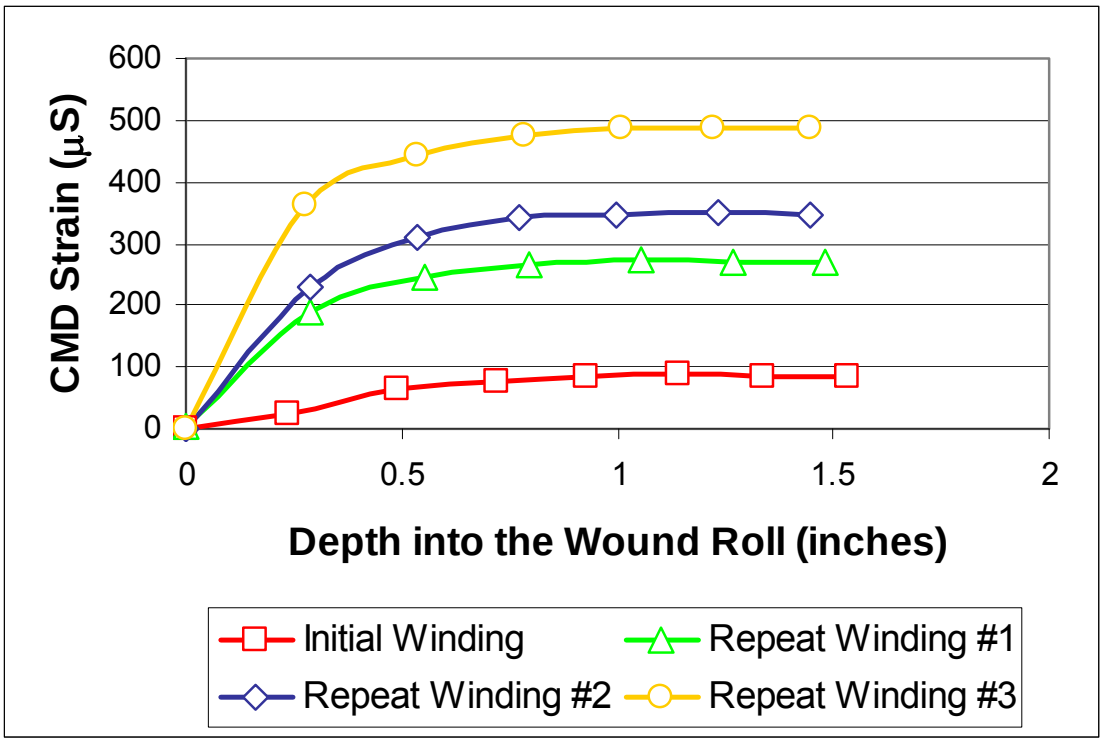

Figure 21: CMD Strains in 24 inch Wide PET

The statistical data is shown in Table 5. The standard deviation of the 24 inch wide material is almost the same as the 6 inch material, but again, is still quite large. Judging by the lack of repeatability seen in Figure 21, this value should be large.

0.25		0.75		1.5	
Mean	201	Mean	289.8	Mean	299.3
Median	209.5	Median	303	Median	313
Standard Deviation	139.6	Standard Deviation	166.7	Standard Deviation	167.7
Range	339	Range	399	Range	403
Minimum	23	Minimum	77	Minimum	84
Maximum	362	Maximum	476	Maximum	487
Count	4	Count	4	Count	4

Table 5: Statistical Results for CMD Strains in 24 inch Wide PET

Finally, the MD strains and CMD strains of the two different widths were compared to one another. The median data sets for each width and each type of strain was chosen. First, the MD strains were evaluated and the plot is shown in Figure 22.

The MD strain of the 6 inch wide web is about 200 μS more than the 24 inch wide web. This is because the stresses involved with the two widths vary so much. While radial stresses are nearly the same for the 6 inch and 24 inch wide webs, tangential stresses and axial stresses differ by quite a lot. The changes in tangential stress contribute to the changes in MD strain for the two widths of material.

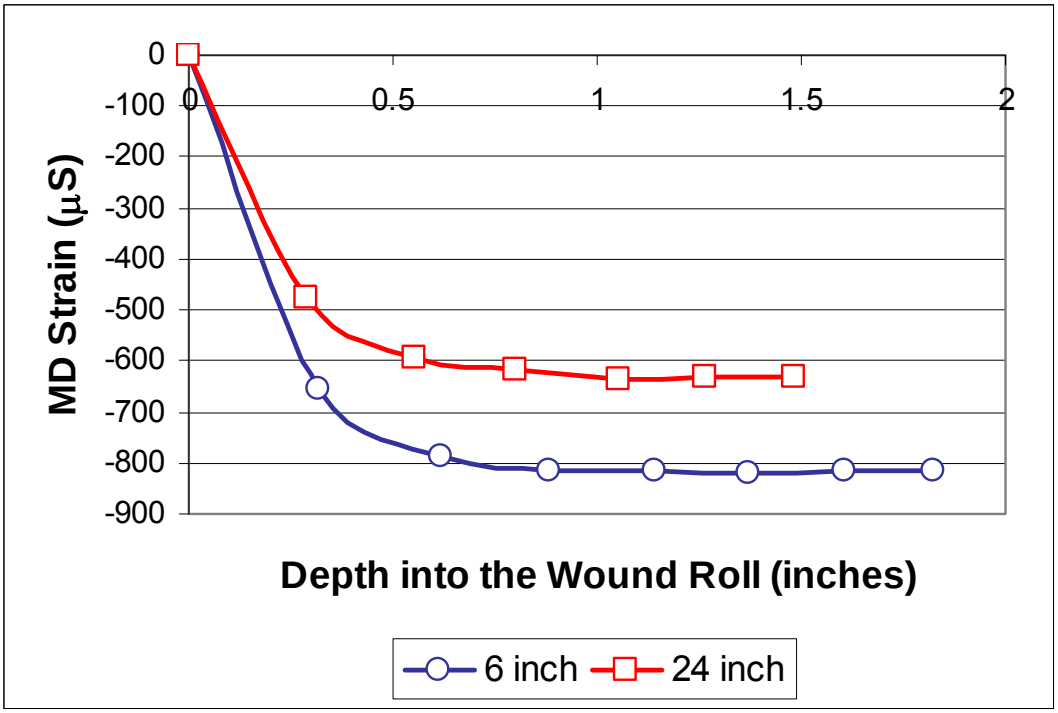

Figure 22: MD Strain Comparison

Just as the MD strains were plotted together, the median CMD strains for the two different widths were plotted together and are shown in Figure 23. In this plot, the median CMD strains of the two different widths are nearly identical. Once again, the axial stresses involved were quite different for the two widths of material. However, since it is CMD strain that is being evaluated now, the strain equation has changed slightly so the difference in axial stress does not appear to have as big an influence on the CMD strain. The range of CMD strain for the 6 inch wide web was approximately 150

µS to 350 µS and for the 24 inch wide web was approximately 100 µS to 500 µS. Therefore, although the median was nearly the same, the range shows the 24 inch wide web had greater CMD strain than the 6 inch wide web.

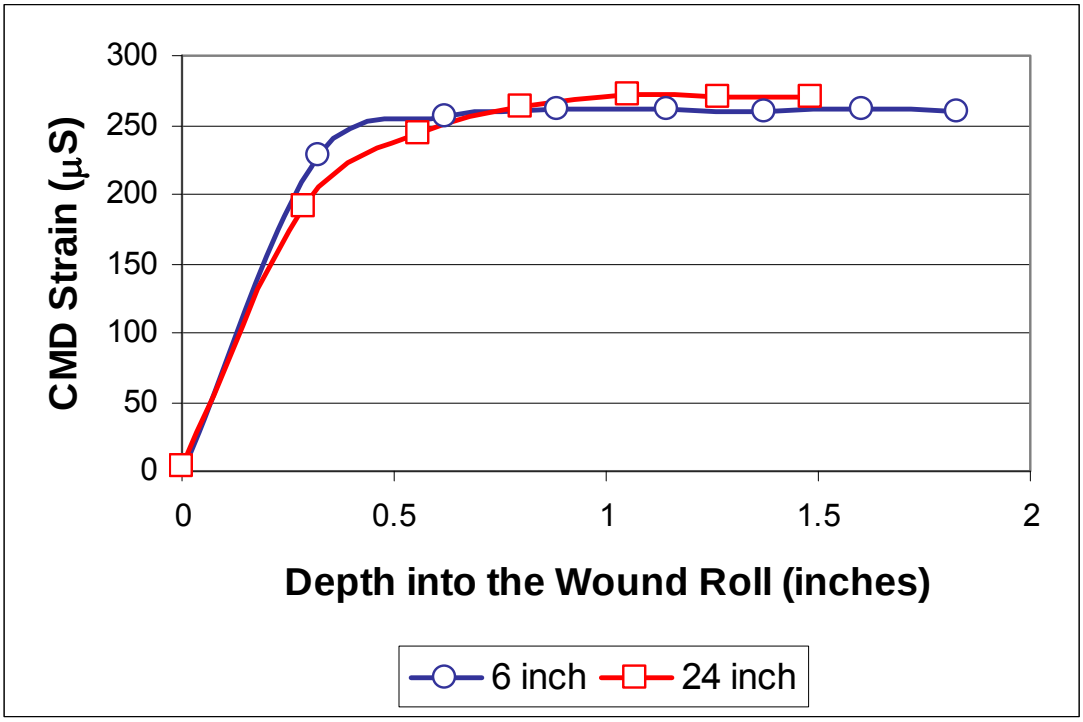

Figure 23: CMD Strain Comparison

In the next chapter, the experimental data discussed in this chapter will be compared to the theoretical data. While the MD strains were quite repeatable throughout the experimental portion of the study, the CMD strains were not. No definitive reasoning was attained for the large range in CMD strain data, but sensitivity to friction was listed as a possible reason. Since the static electricity produced when winding the rolls was somewhat great, it could have been great enough to produce enough friction in the web to give the range seen in the CMD strain data.

CHAPTER VI

COMPARISON OF MODEL AND EXPERIMENTAL RESULTS

The experimental strains that were measured experimentally must now be verified using the two-dimensional model described in Chapter 3. The axisymmetric winding code output the stresses, radial, tangential, and axial, found in the wound roll. This data had to be manipulated into strains so that it could be compared to the experimental data that was taken.

For each experimental data point recorded, a theoretical data point was created from the axisymmetric code. The material properties described in Chapter 3 were input and an Excel file was generated for each run of the axisymmetric code. The only parameter that changed in each successive run of the code was the roll radius. There were eight codes run for each width of material. As stated in Chapter 4, with each strain recording, the pile height of the roll was taken as well. This pile height was converted into a radius value by adding the radius of the core which could then be input in the axisymmetric code. The eight radius values chosen for the code inputs were simply averages of the experimental radius values at each pile height recorded for the tests used in this study. Each experimental strain recorded in each experiment had approximately the same pile height value. For the 6 inch wide web, the radius values, in inches, used for input to the code were 3.16, 3.46, 3.75, 4.04, 4.27, 4.5, 4.7, and 4.94. For the 24 inch

wide web, the radius values, in inches, used for input to the code were 3.64, 3.91, 4.17, 4.41, 4.64, 4.86, 5.07, and 5.51.

After the results were interpreted by the code, the strains could be calculated from the stress values output by the axisymmetric code into an Excel file. The Excel file reported three stresses; radial stress, σ_r, tangential stress, σ_θ, and axial stress, σ_z. Each of these stresses was reported in six different segments across the width of the wound roll. The only stress evaluated for comparison to the experimental data was at segment 3, or at the centerline of the wound roll, which saw the greatest amount of stress and was closest to the location where the strain data was collected experimentally.

These stresses were used to produce machine direction and cross machine direction strains using the following equations:

$$\varepsilon_\theta = \frac{-\nu_{\theta r}}{K_2 \cdot \left(-\sigma_r + K_1\right)} \cdot \sigma_r + \frac{\sigma_\theta}{E_\theta} - \frac{\nu_{\theta z}}{E_z} \cdot \sigma_z \quad , \tag{6.1}$$

$$\varepsilon_z = \frac{-\nu_{zr}}{K_2 \cdot \left(-\sigma_r + K_1\right)} \cdot \sigma_r - \frac{\nu_{z\theta}}{E_\theta} \cdot \sigma_\theta + \frac{\sigma_z}{E_z} \quad , \tag{6.2}$$

The theoretical strains were calculated for each radius at which an experimental reading was taken. The strain at the radius at which the gage was inserted was subtracted from each successive radius value. This simulated the balancing procedure that was used in the experimental procedure. The following equations show the subtraction method used:

$$\varepsilon_\theta = \varepsilon_\theta(r) - \varepsilon_\theta(\text{gage}) \quad , \tag{6.3}$$

$$\varepsilon_z = \varepsilon_z(r) - \varepsilon_z(\text{gage}) \quad , \tag{6.4}$$

where $\varepsilon_\theta(r)$ and $\varepsilon_z(r)$ are the strains at the radius being evaluated and $\varepsilon_\theta(gage)$ and $\varepsilon_z(gage)$ are the strains at the radius at which the gage was attached.

One difference between the experimental strain values plotted in this chapter and the ones plotted in Chapter 5 is that the negative bending strain was added to the strain reading taken experimentally. This was done because of the balancing process in the experimental procedure as described in Chapter 4. The bending strain was a calculated value, based on the thickness of the web material at the location that the strain gage was attached and thus, readings were being taken. The equation used for bending strain is shown below.

$$\varepsilon = \frac{Y}{R}, \tag{6.5}$$

The Y value calculated included the thickness of the strain gage that was attached to the web. A diagram of the bending strain calculation is shown in Figure 24. The line marked NA, neutral axis, is the line where the length before and after bending is the same and can be used as a reference to determine the strain in other areas of the bent segment. The only area of interest in this case would be the outside of the web layer. The radius of curvature is marked R and completes the relation between strain to the distance, Y, from the neutral axis and the radius of curvature, R.

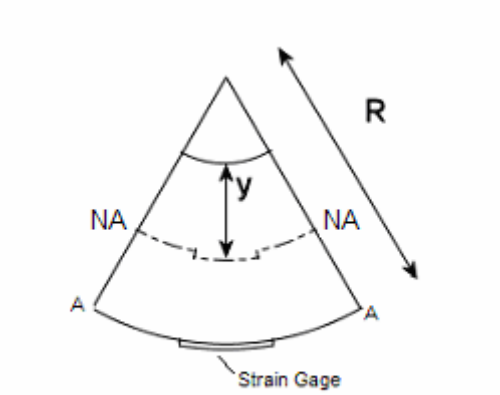

Figure 24: Bending Strain Diagram

The thickness of the strain gage was taken with a set of digital micrometers and confirmed with information provided about the strain gage from the manufacturer. The single element gage was 0.0025 inches thick and the rosette gage was 0.003 inches thick.

Figure 15 in Chapter 4 showed where the strain gage was attached and balanced in the roll. Since the gage was attached on a curved surface and then balanced, the bending strain was balanced out. Ideally, only the changes in membrane strain should have been measured. The circumferential membrane strains due to winding are decreased as the strain gage is wound down into the roll. However, these changes in membrane strains did not match the strains from the model. The difference between the two was roughly the negative of the calculated bending strain from Equation 6.5. The only way the bending strain could have become negative is if after the installation and balancing of the gage, it was subject to something that caused it to have less radius of curvature instead of more as laps were added onto the roll during winding. It is assumed that the gage did not conform to the roll radius when it was installed and winding further laps on top of it caused the radius of curvature to decrease. This would give a negative

bending strain that could be added to the already negative changes in membrane strain to give the strains seen in the model.

The experimental data was previously presented as strain as a function of the depth in the wound roll. The theoretical data was presented in Chapter 3 as stress as a function of radius of the wound roll. This theoretical data needed to be converted from stress to strain and then from radius to depth in the wound roll.

First, the stresses reported in Chapter 3 were converted to MD and CMD strains as a function of wound roll radius. Stress data from segment 3 of the 6 inch and 24 inch wide rolls were used to calculate the MD and CMD strains from Equations 6.1 and 6.2. The 6 inch wide web strains are shown first. Figure 25 shows the MD strain as a function of wound roll radius. Since segment 3 showed the highest tangential stresses, as discussed with Figure 7 in Chapter 3, the strains shown in Figure 25 are also the highest in the width of the roll. The strains shown represent the strains at the centerline of the roll so a comparison could be made with the experimental data, which was taken at the centerline of the roll.

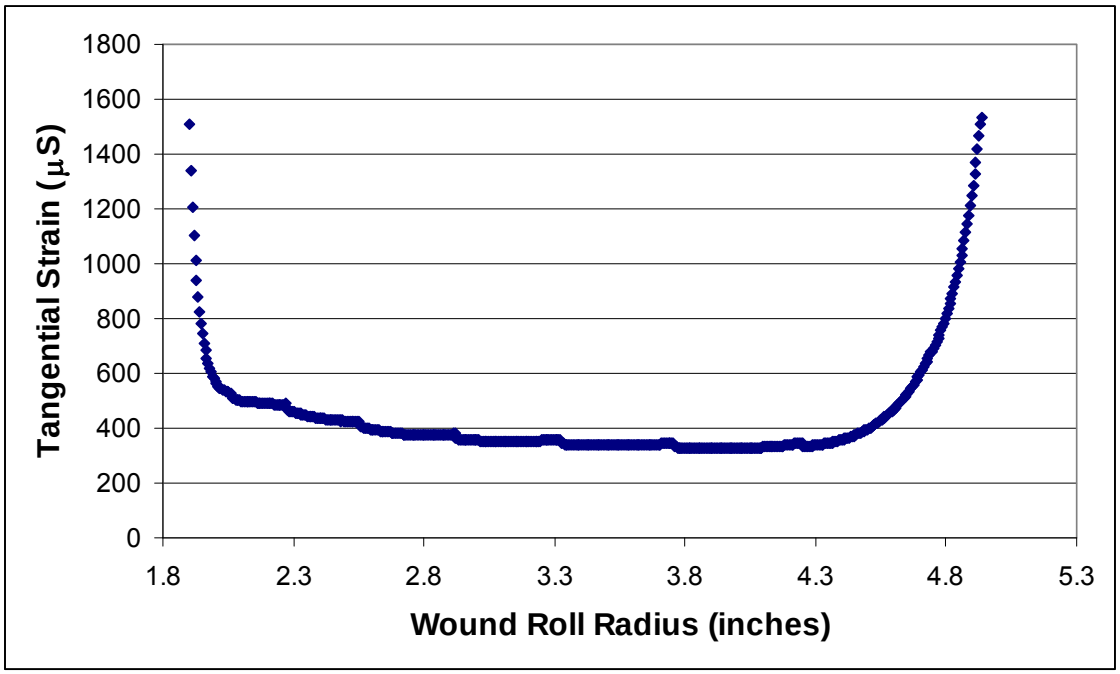

Figure 25: MD Strain for 6 inch Wide Web

Figure 26 shows the CMD strain as a function of wound roll radius. Once again, since segment 3 is being plotted, the CMD strains shown are the highest in the width of the roll of material.

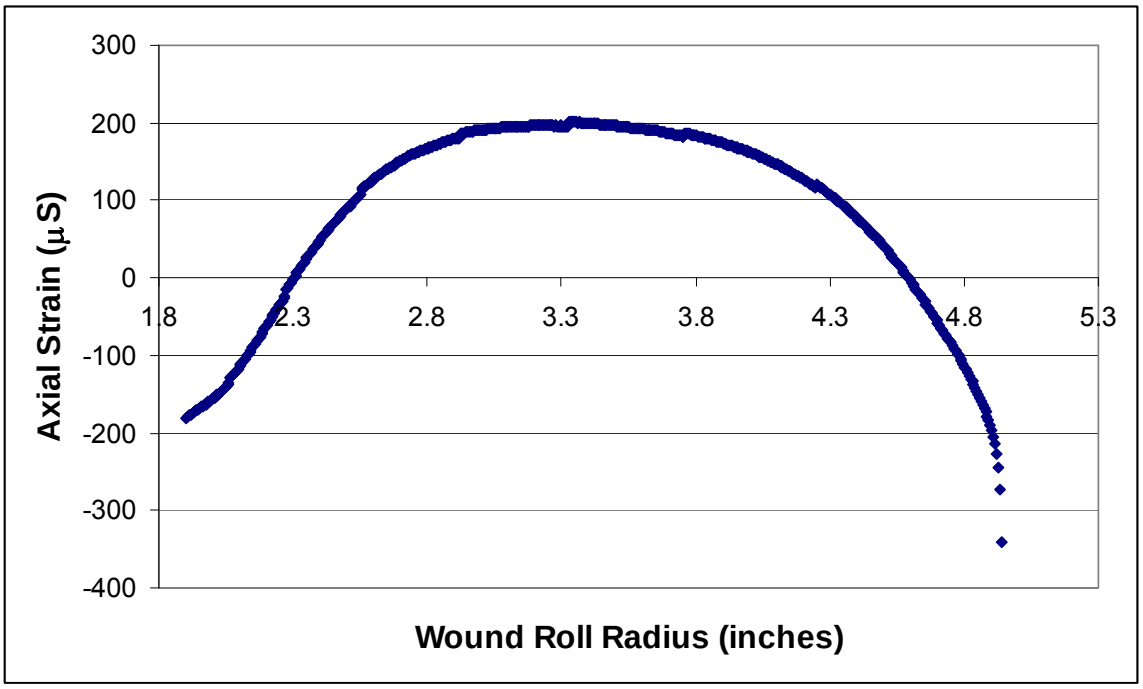

Figure 26: CMD Strain for 6 inch Wide Web

Now, the 24 inch wide web stresses are converted to strains. Figure 27 shows the MD strain as a function of wound roll radius. MD strains for the 24 inch wide web were similar to the MD strains in 6 inch wide web. The 24 inch wide web saw slightly less MD strain within the winding roll than the 6 inch wide web saw.

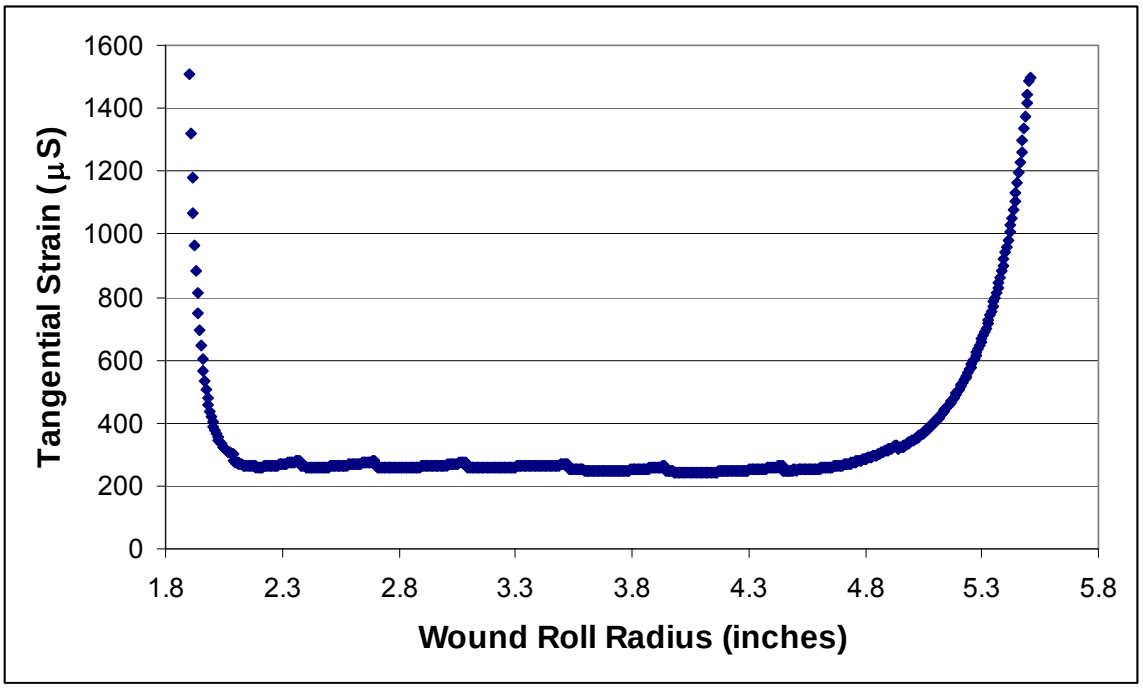

Figure 27: MD Strain for 24 inch Wide Web

Figure 28 shows the CMD strain as a function of radius. CMD strains for the 24 inch wide web are very different from CMD strains for the 6 inch wide web. This was also seen when comparing the axial stresses of the two different widths. The CMD strain of the 24 inch wide web is so different from the CMD strain of the 6 inch wide web because it is approaching plane strain, whereas the 6 inch wide web is not.

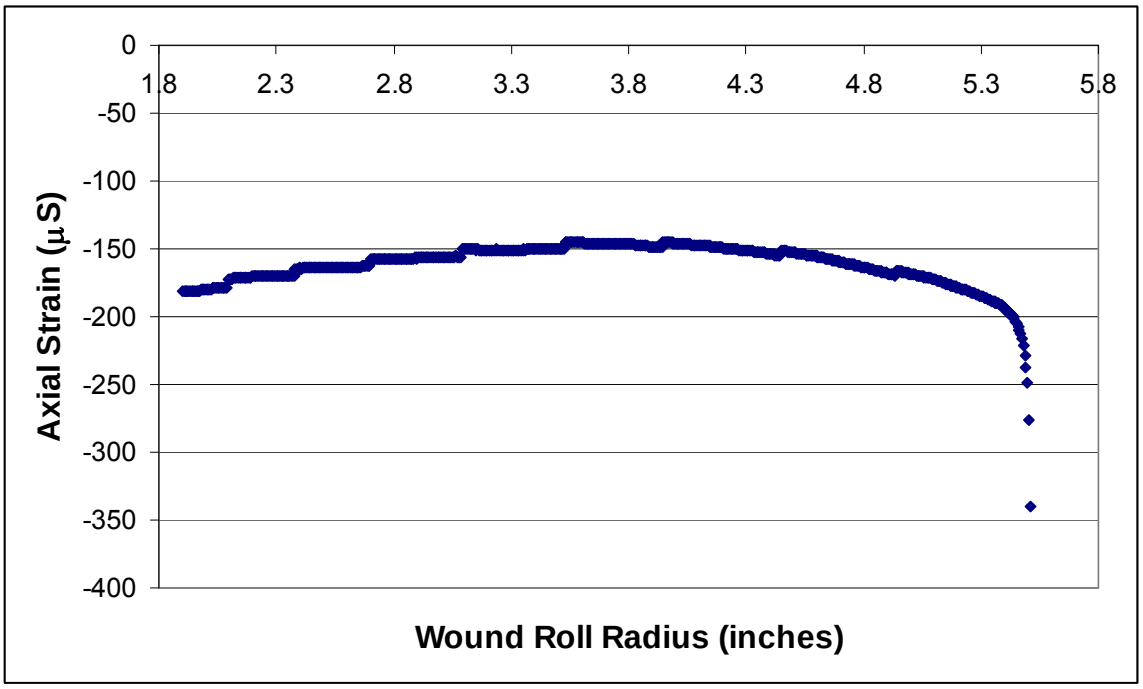

Figure 28: CMD Strain for 24 inch Wide Web

Next, the radius of the wound roll was converted to depth in wound roll. This was a fairly easy conversion. The radius at each data point was subtracted from the final radius of the wound roll. Figure 29 shows an example of this shift. This plot corresponds to Figure 27. The outside of the wound roll is now shown at a depth of 0 inches and the strain gage attachment is shown at a depth of approximately 3.5 inches. This same conversion was done for the three other strains plots that were presented in this chapter.

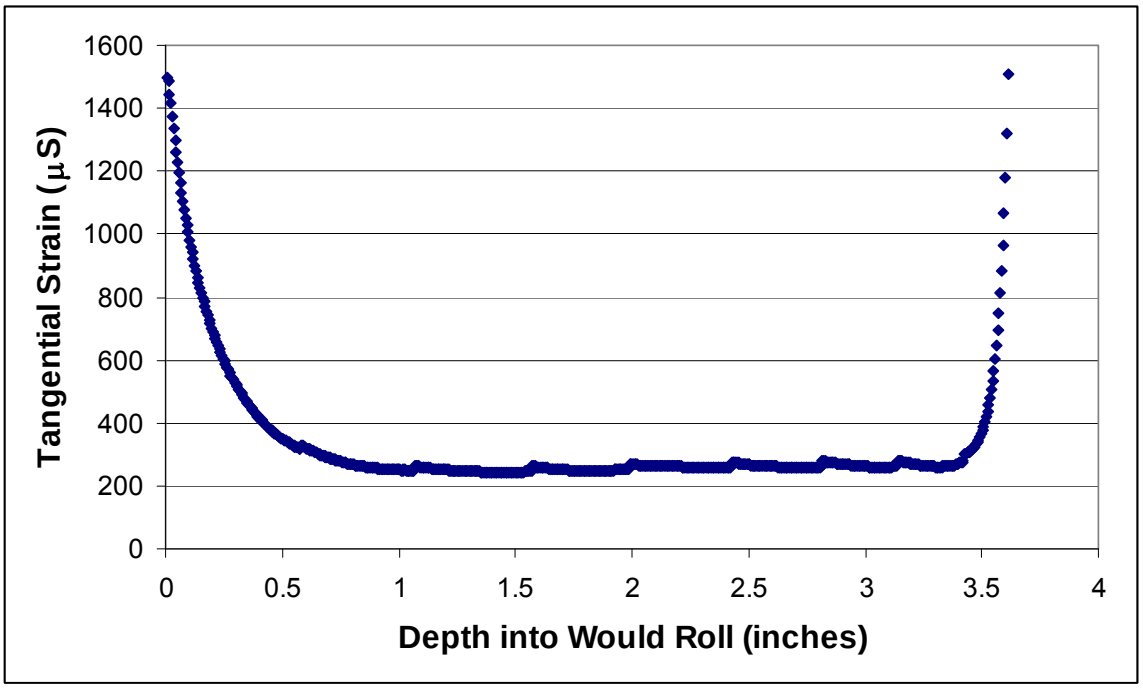

Figure 29: Depth of Gage in Wound Roll Example Plot

All of the theoretical plots are now in the form of strain as a function of depth in the wound roll, but the strains shown are for the final wound roll radius. As discussed earlier in this chapter, there were several codes accomplished for each width of web material. The strain at the depth at which the strain gage was attached had to be subtracted from the strain at each successive depth. Doing this simulated the balancing method that was accomplished in the experimental procedure so that the theoretical and experimental results could be plotted and compared on the same scale.

Figure 30 shows the final theoretical MD strain for comparison to the experimental results. As previously discussed, the eight average radius values that were chosen to compare to the experimental results are obvious here and shown as depth in the wound roll. In this way, the theoretical and experimental results can be compared on the same scale.

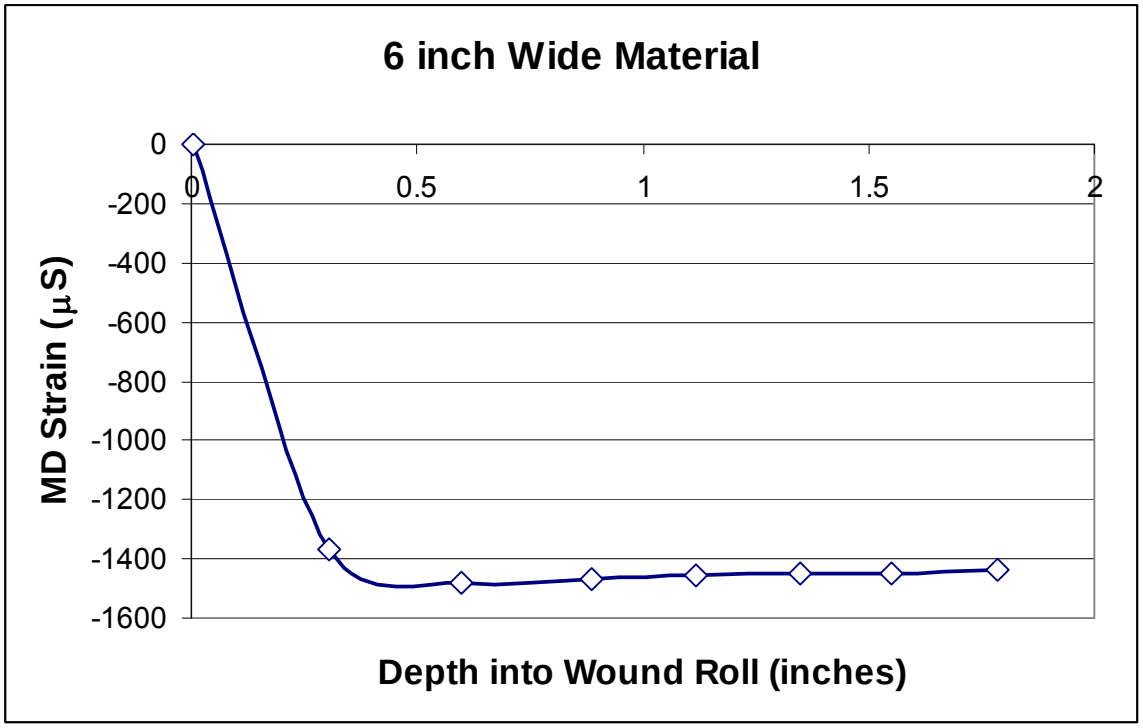

Figure 30: MD Strain for 6 inch Wide Web for Comparison with Experimental Results

The next three figures show the remaining theoretical plots for comparison to the experimental data. Figure 31 shows the theoretical CMD strain for the 6 inch wide web, while Figure 32 and Figure 33 show the MD and CMD strains for the 24 inch wide web. As discussed previously, the 24 inch wide web is neither in plane stress or plane strain, so the CMD strain plot differs from the CMD strain plot of the 6 inch wide web considerably.

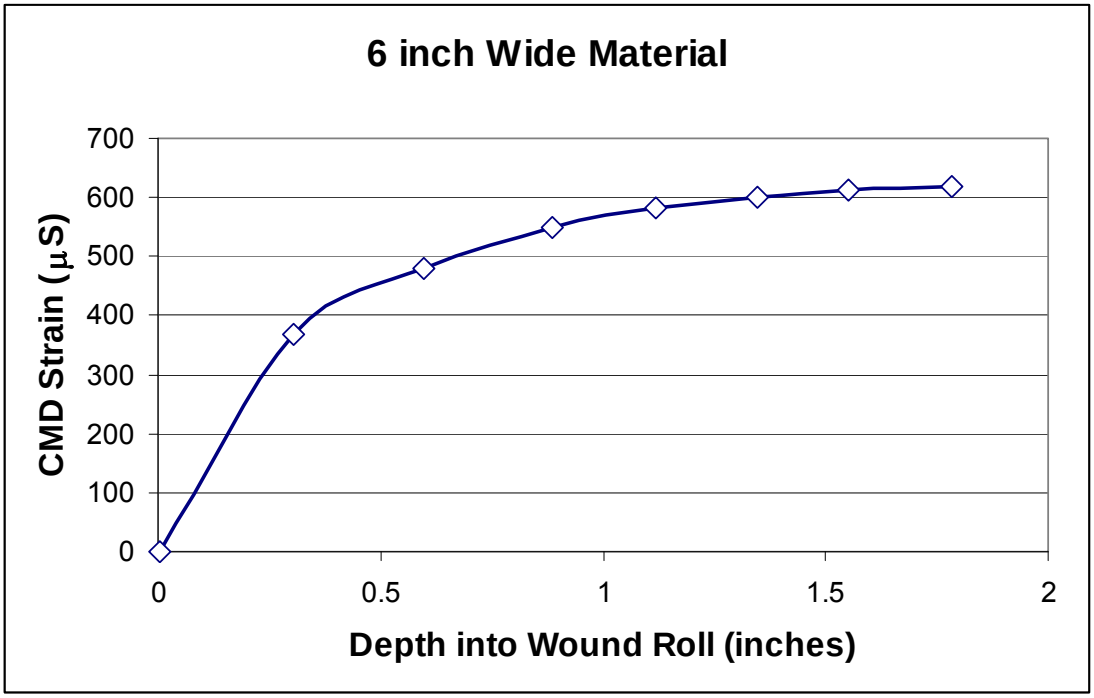

Figure 31: CMD Strain for 6 inch Wide Web for Comparison with Experimental Results

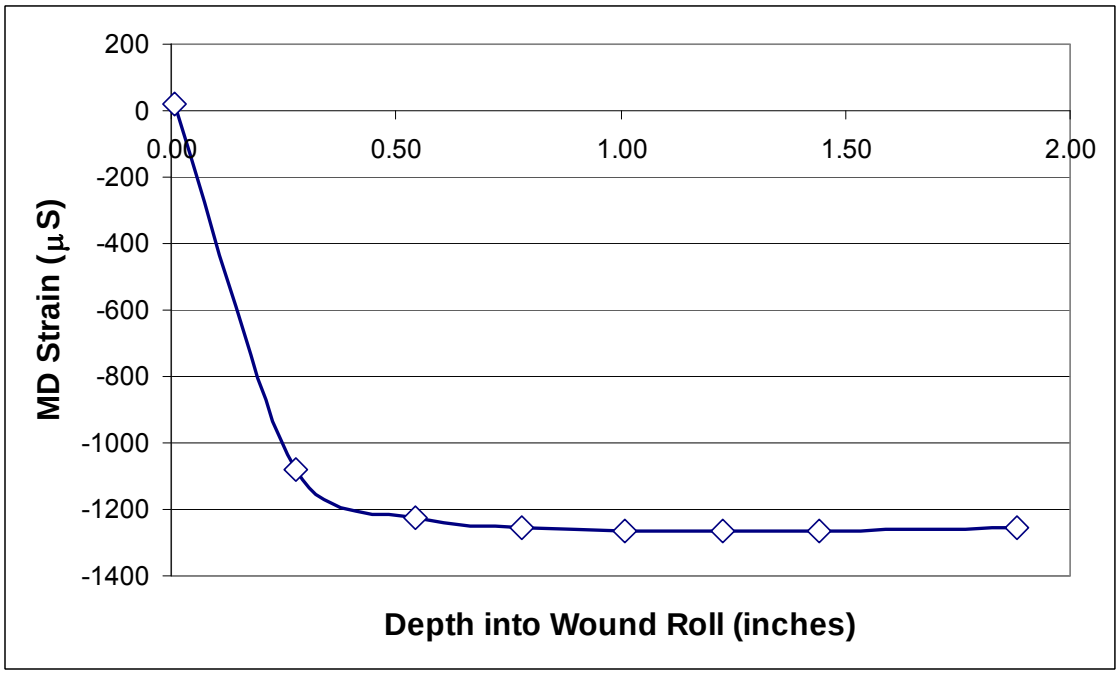

Figure 32: MD Strain for 24 inch Wide Web for Comparison with Experimental Results

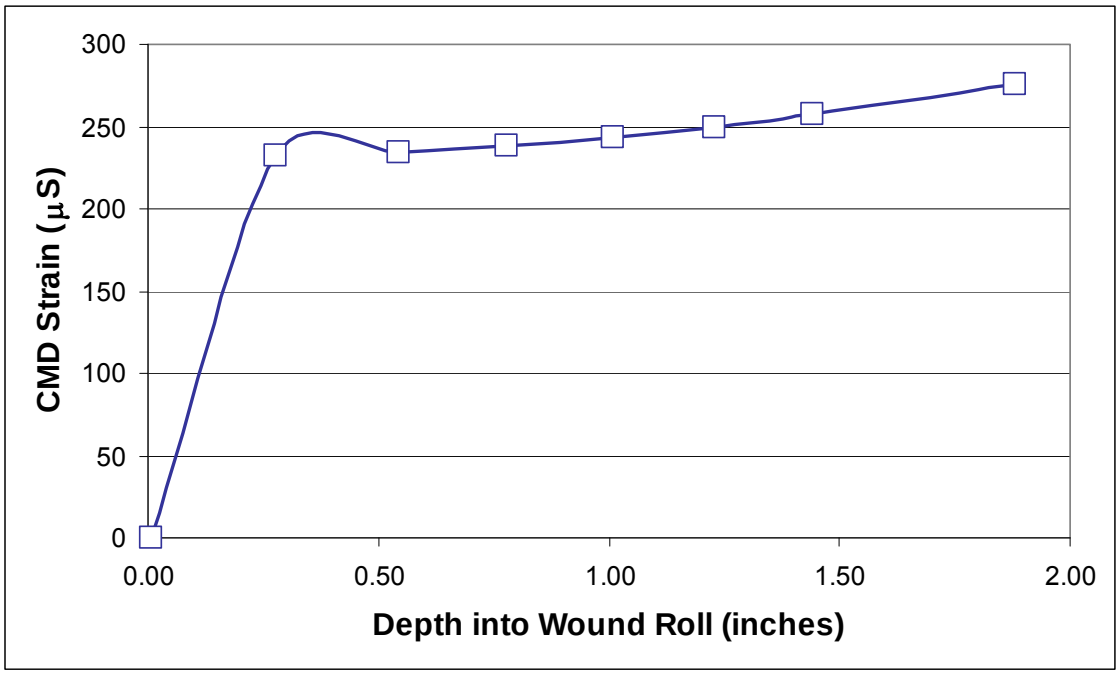

Figure 33: CMD Strain for 24 inch Wide Web for Comparison with Experimental Results

It should be noted that in Figure 33, the data appears to jump up between the second and third data point. There is no reason for this. When plotting data points in Excel, sometimes Excel chooses an arbitrary point to connect to. There is no point in the data between the second and third points that is higher than either of those two points. This will be seen again when comparing the theoretical data to the experimental data and the same explanation holds.

Now, the theoretical data could be plotted with the experimental data to confirm the results of the model. Figure 34 shows the comparison of the theoretical and experimental MD strains for the 6 inch wide web. In this case, the experimental data match quite well with the theoretical data, which is shown as a solid black line. The experimental data did exhibit slightly more strain than the strains predicted by the model.

Taken at approximately 1.0 inch of depth into the wound roll, the percent difference between the theoretical data and the experimental data ranged from 6.4% to 14.4%.

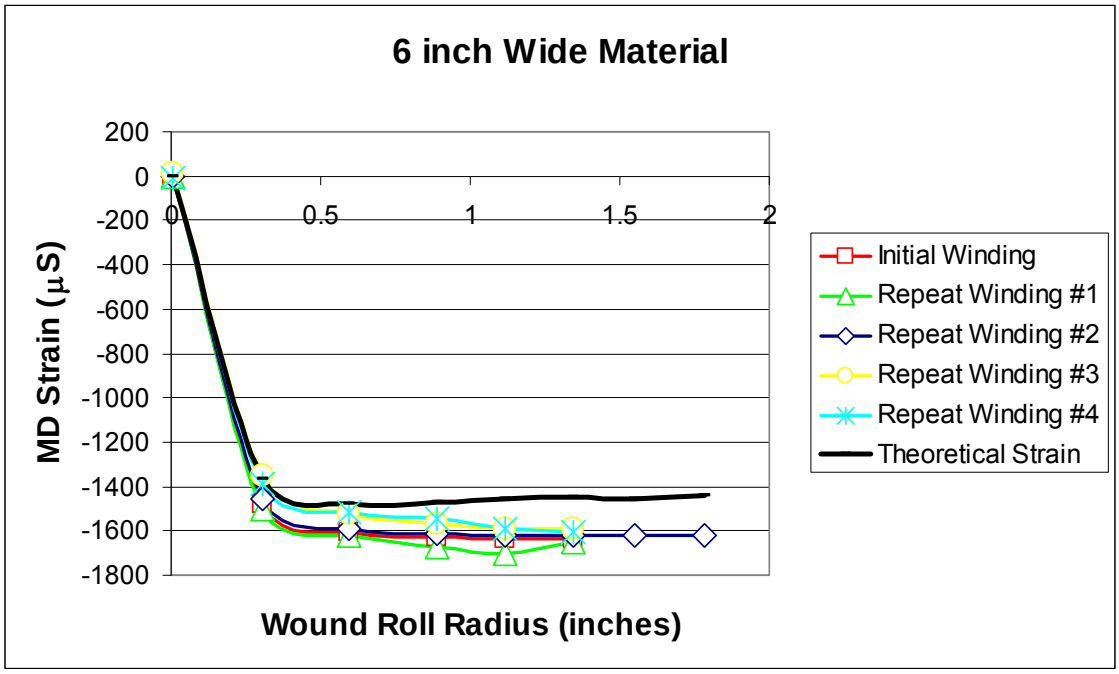

Figure 34: Theoretical and Experimental MD Strains for 6 inch Wide Web

Figure 35 shows the comparison of the theoretical and experimental CMD strains for the 6 inch wide web. As discussed previously, the experimental CMD strains varied much more than the MD strains. The theoretical CMD strain is on the higher end of the experimental data. The percent differences between theoretical and experimental CMD strain ranged from 3.2% to 115.6%. Since the CMD strains varied so much, the percent differences were bound to be much more erratic than the percent differences for the MD strains.

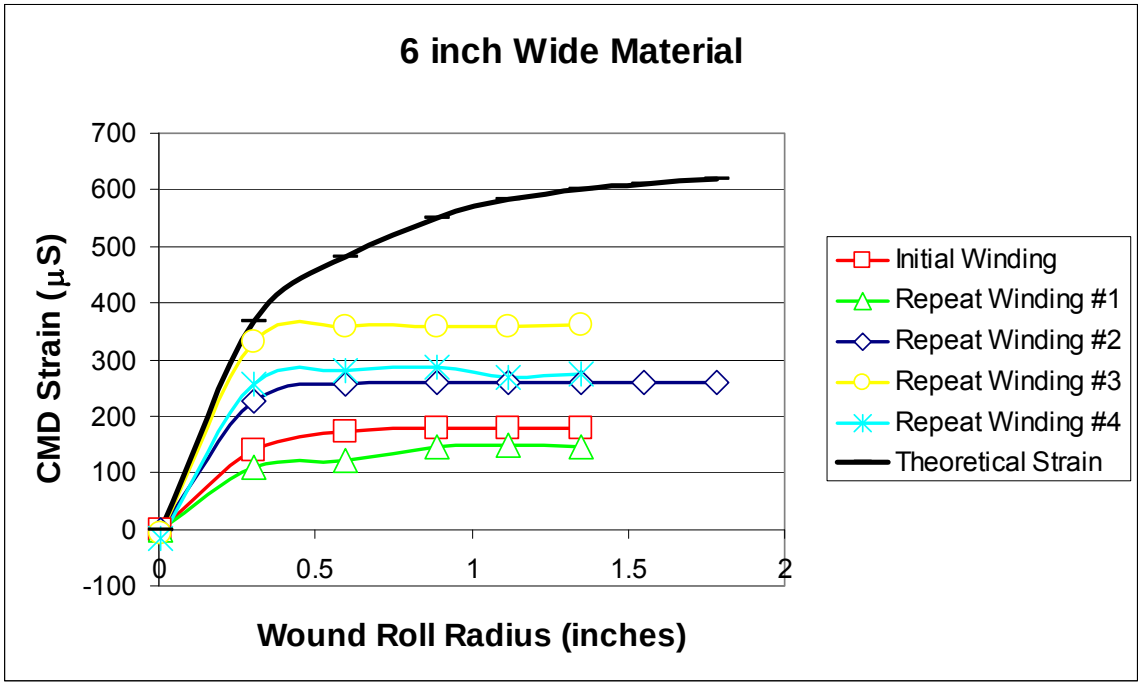

Figure 35: Theoretical and Experimental CMD Strains for 6 inch Wide Web

Figure 36 shows the comparison of the MD strain for the 24 inch wide web. This time, the experimental strains showed up on both sides of the theoretical strain line. The percent difference between the experimental and theoretical MD strains ranged from 5.4% to 17.6%. The percent difference results were similar to the results found in the MD strain for the 6 inch wide web.

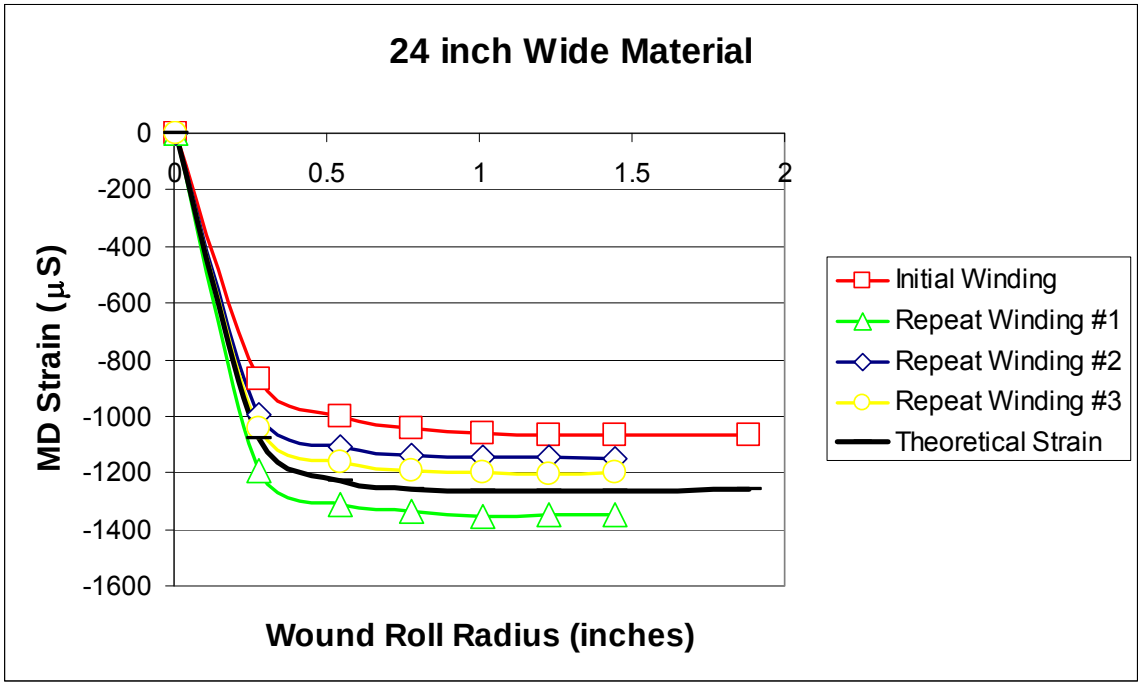

Figure 36: Theoretical and Experimental MD Strains for 24 inch Wide Web

The final comparison is the comparison of the CMD strains for the 24 inch wide web. Figure 37 shows this comparison. The percent differences between theoretical and experimental CMD strain ranged from 11.2% to 98.1%. Just as the CMD strains in the 6 inch wide web showed high percent differences, these CMD strains show high percent difference as well. The percent difference results for the two different widths of material were, again, similar for the CMD strains.

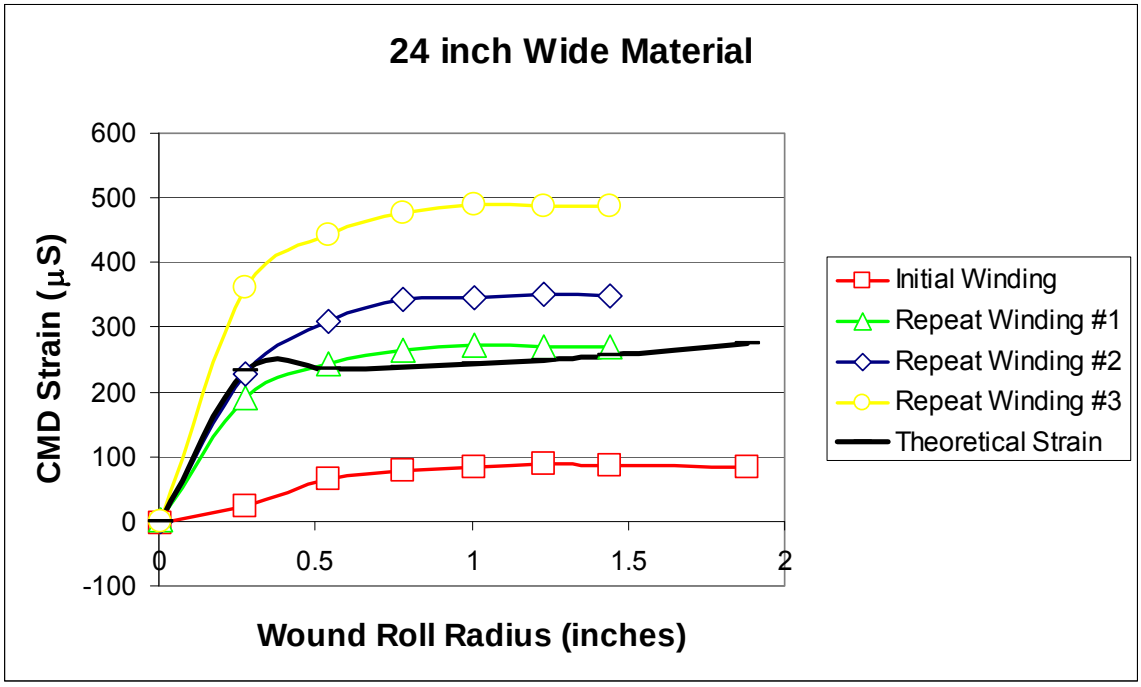

Figure 37: Theoretical and Experimental CMD Strains for 24 inch Wide Web

There were a number of experimental tests performed to compare to the theoretical data from the model. Now, an average of the experimental data points was taken and that average experimental data was compared to the theoretical data so that an average comparison could be made.

Figure 42 shows the first comparison. Standard deviation bars on the average experimental data show that the averaged tests were close together and very repeatable. The percent difference between theoretical and average experimental MD strain taken at a depth of 1.0 inch was 8.8%. This average data was quite close to the theoretical data predicted by the model.

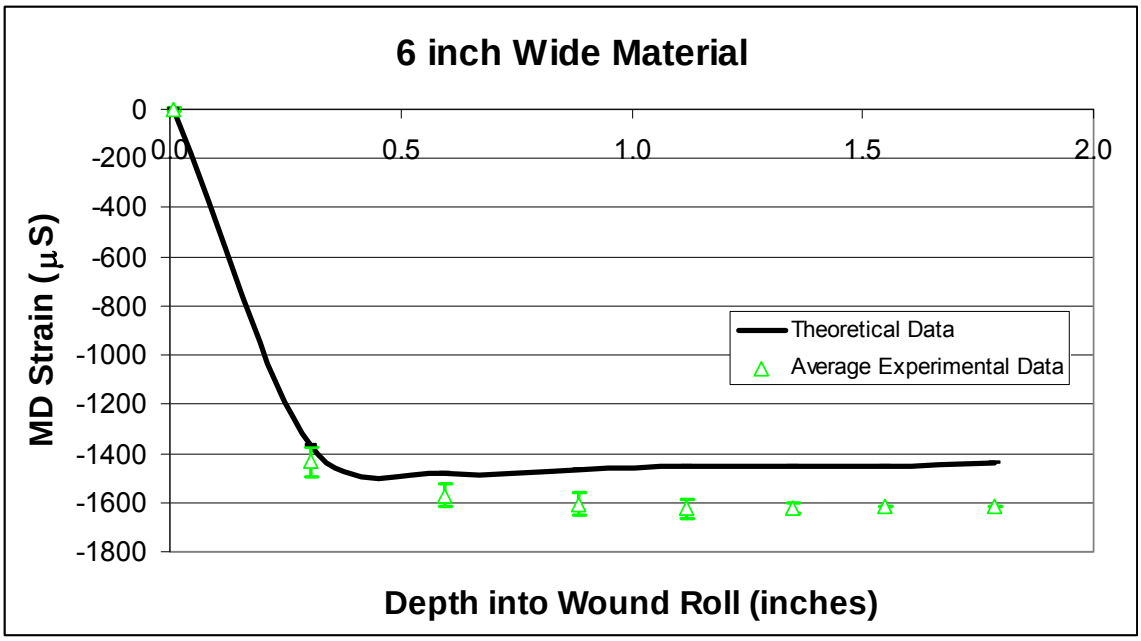

Figure 38: Theoretical and Average Experimental Comparison of MD Strains for 6 inch Wide Web

Figure 43 shows the next comparison of CMD strains. Standard deviation bars in this plot are a little greater than in the MD strain data. The percent difference between theoretical and average experimental CMD strain taken at a depth of 1.0 inch was 58%. This average data did not really compare to the theoretical data that was output by the model. Thinking back to Figure 39, the experimental CMD data was not grouped together nicely as it was with the MD data, so it made sense that the average experimental data would not closely match the theoretical data.

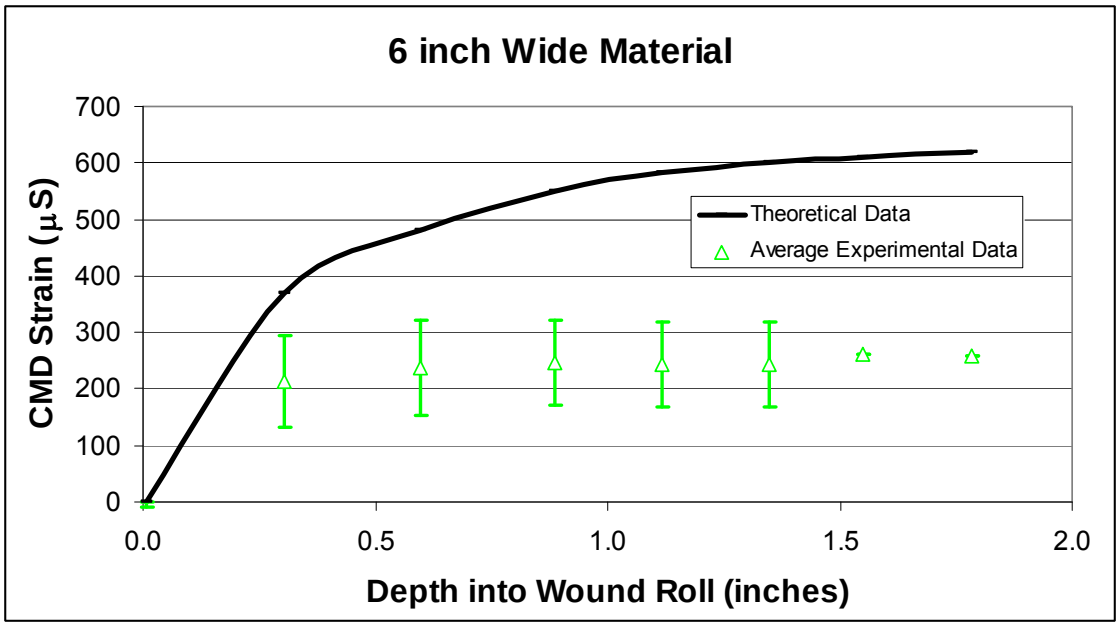

Figure 39: Theoretical and Average Experimental Comparison of CMD Strains for 6 inch Wide Web

Figure 44 shows the next comparison for MD strain, this time for the 24 inch wide web. Standard deviation bars show the averaged tests were grouped together nicely and quite repeatable. The percent difference between theoretical and average experimental MD strain taken at a depth of 1.0 inch was 6.1%. Again, this average data matched quite well with the theoretical data output by the model.

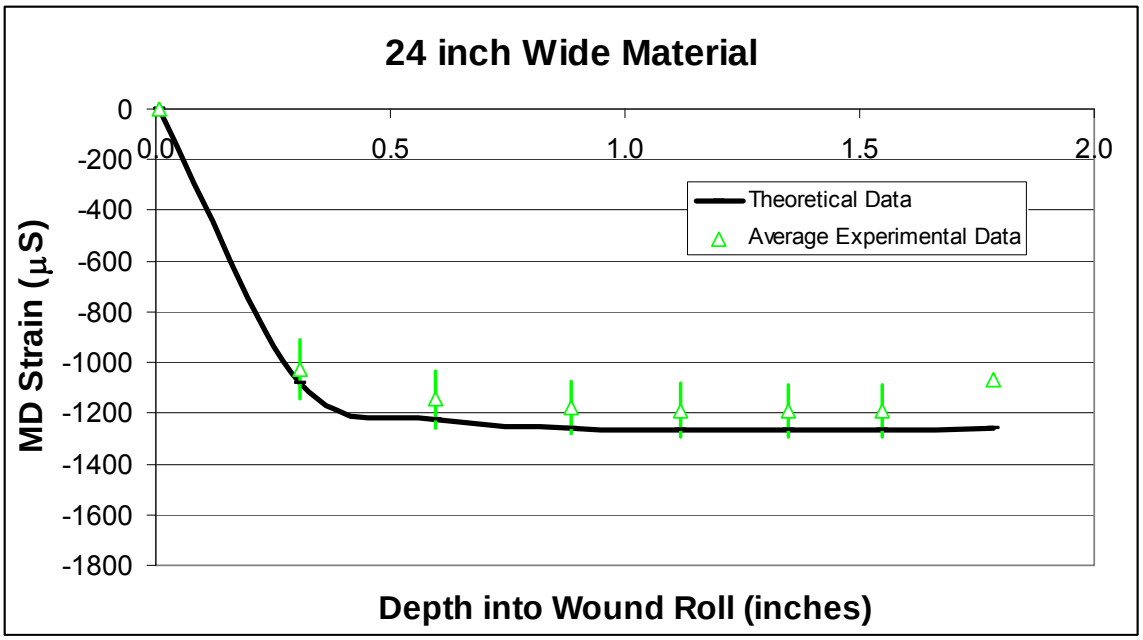

Figure 40: Theoretical and Average Experimental Comparison of MD Strains for 24 inch Wide Web

The last average figure for comparison is Figure 45, which shows the average CMD strain comparison for the 24 inch wide web. The standard deviation bars show about the same standard deviation as was seen in the MD data for the 24 inch wide roll. The percent difference between theoretical and average experimental MD strain taken at a depth of 1.0 inch was 20%. This percent difference is much better than what was seen in the 6 inch wide web, but still further off than the MD strain data.

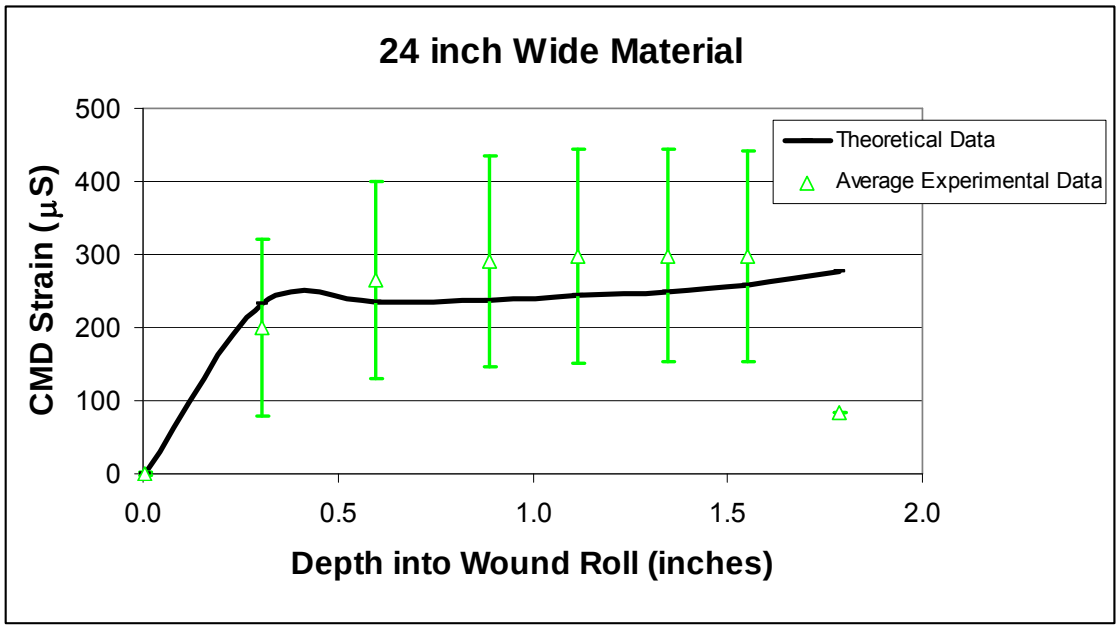

Figure 41: Theoretical and Average Experimental Comparison of CMD Strains for 24 inch Wide Web

The results presented in this chapter represent a total of nine of the experiments that were performed in all. Data not presented in this chapter was not accurate because of improper testing procedures and/or user error. The final chapter will draw the necessary conclusions for this study.

CHAPTER VII

CONCLUSIONS

In Chapter 1, the topic of this study was introduced as the study of the development of axial stresses in wound rolls. These axial stresses were first calculated by a two-dimensional winding model and then were verified by performing in lab experiments on wound rolls. Strain measurements were taken in the wound rolls by attaching a strain gage(s) at a certain radius and connecting it to a strain indicator to give the measurement.

In Chapter 2, research about stress in wound rolls was covered. While many researchers have been studying stress and strain in wound rolls for quite some time now, the winding models that predict axial stresses have never been verified. In short, this study set out to do just that. The next few chapters covered the discussion of the winding model and the experimental procedure. While several mistakes were made in collection of data, there were plenty of tests available to extract data from so that verification of the model outputs was possible.

In Chapter 6, the experimental data was compared to the theoretical data. Using this information, it can be said that the research objective was partially satisfied. From the work produced in this study, the models are making a good estimate of the axial

stresses in the wound rolls. The theoretical MD strains for both widths of material tested were close to the experimental strain obtained when bending strains were subtracted from the measured strain value. The CMD strains were harder to match to the theoretical strains. Additionally, the CMD strain in the 6 inch wide web was the least accurate while the CMD strain for the 24 inch wide web was a little more accurate. While no definitive reason was given, the high amount of static electricity was listed as a possible cause for increasing friction in the wound roll. The CMD strains could have been more sensitive to the friction caused by the static electricity.

The best agreement occurred in the 24 inch wide material for both MD and CMD strains. The 24 inch wide roll was close to achieving plane strain conditions at the widthwise center line of the roll at all radial locations. This was not true for the 6 inch wide roll where the axial stresses diminished to zero at the intermediate wound roll radial locations. Thus, it may follow that the model may be predicting the winding stresses and strains more accurately for cases where near plane strain conditions exist.

Conclusions

In Chapter 1, the research objectives were stated. The first goal was to verify the axisymmetric winding model and the second goal was to determine if the axial stresses were sufficient to cause corrugations. These two objectives will be revisited here.

The experimental results for MD strain seemed to match the theoretical results of MD strain as calculated from the stress output of the axisymmetric code when calculated bending strains were added back into the experimental strains. The percent differences between the MD strains and the calculated theoretical strains were quite low and further indicated that the model was verified for the prediction of MD strains. This agreement

was made possible by adding a negative bending strain component to the test values of MD strain. While no quantitative explanation can be given for this, it is believed this was the result of bending of the gage due to increased thickness of the web in the region where the gage was bonded. As additional layers of web were wound onto the roll, this induced a compressive bending strain in the outer surface of the strain gage. This worked well for both the 6 inch and 24 inch wide rolls as shown in Figures 38 and 40.

The gages mounted in the CMD direction should have been insensitive to the bending strains in the MD direction, therefore these experimental strains were not corrected by a bending strain component. The experimental results for CMD strain matched closely in shape of plot, but values were further off mark. The CMD strain for the 6 inch data was the biggest problem. While static electricity was generated in the material during winding, this could not be the only solution especially since even more static electricity was generated during the winding of the 24 inch wide material and CMD data for the 24 inch wide web was a closer match to the theoretical data. It appeared that plane strain conditions were achieved for the 24 inch wide roll, but not the 6 inch wide roll at the roll center line where the strain gage was applied. For cases where plane strain conditions exist, such as the 24 inch wide roll, the model is verified.

The second research objective was to establish if the axial stresses that were associated with winding were sufficient to cause corrugation failures. While corrugations were of interest in this study, they were not specifically being studied in the laboratory. The point was the documentation of the axial stresses involved in winding, not the producing corrugations. A conservative value of critical axial stress is defined by the following equation [18]:

$$\sigma_{CMDcritical} = \frac{-t}{r} \cdot \frac{E_{MD}}{\sqrt{3\left(1 - \upsilon_{\theta z}^{\,2}\right)}}, \qquad (7.1)$$

Therefore, the critical stress for the 6 inch wide web was -174 psi and for the 24 inch wide web was -156 psi. When calculating these values, a radius of 4.94 inches was used for the 6 inch wide roll and a radius of 5.51 inches was used for the 24 inch wide roll. All other parameters were constants that are found in Table 1.

Based on the axial stress data from the winding code, the critical stress can be compared to data from the winding model. In the 6 inch wide web, the critical axial stress of -174 psi was reached at the beginning of the winding roll where the core and web material were being modeled as one. The rest of the winding was below the critical value and only approached it again at the end of the winding roll. In the 24 inch wide web, the critical axial stress of -156 psi was reached and exceeded at the beginning of the winding process and continued to be greater than the critical value until winding was over.

According to this analysis, the axial stresses produced in the 6 inch wide web were great enough to produce corrugations at the start of winding, but no where else in the roll. In the 24 inch wide web, the axial stresses were great enough to produce corrugations throughout the winding roll, although none were witnessed during the experimental portion of the study. The critical axial stress equation used did not account for the stiffness of the web material that was supporting the outer layer of the wound roll. Therefore, the real critical axial stress value would be much higher and explains why no corrugations were seen when winding.

Future Work

More work should be done on the experimental collection of the CMD strains. Better experimental techniques should be developed to obtain strain values experimentally. When looking at all the MD and CMD strains obtained experimentally in the appendix, the results were quite scattered. The cause of this could be from multiple sources, but better experimental techniques would alleviate at least some of the scatter in the data. It is suggested that strain gages be mounted both inside and outside the lap under study and connect into opposing arms of a Wheatstone bridge to actively cancel all bending strain components. This should be done for the gage mounted in the CMD direction as well.

More research should also be done to determine why the 24 inch wide web produced more favorable results of CMD data than the 6 inch wide web produced. Additionally, new critical axial stress equations should be studied to account for the stiffness of the core and give a more accurate critical axial stress with which to compare the model. This study focused on axial stresses and their effect on the wound roll, but other sources of two direction stress should be studied to determine their potential effect on the roll as well.

This study focused on center winding of PET film at 0.002 inches thick and at two different widths. Further testing of other materials at alternate widths and thicknesses would be a good idea to further validate the model. Additionally, other forms of winding should be tested to verify the model. Another interesting study may be to use the two-dimensional winding model used in this study to explore diameter to width ratios

combined with the material properties which will lead to plane strain conditions throughout the roll.

REFERENCES

1. Hakiel, Z., "Nonlinear Model for Wound Roll Stresses," *Tappi Journal*, Vol. 70, No. 5, May 1987, pp. 113-117.
2. Cole, K. A. and Z. Hekiel, "A Nonlinear Wound Roll Stress Model Accounting for Widthwise Web Thickness Nonuniformities," *AMD*, Vol. 149, 1992, pp. 13-24.
3. Lee, Y. M. and J. A. Wickert, "Stress Field in Finite Width Axisymmetric Wound Rolls," *Transactions of the ASME*, Vol. 69, March 2002, pp. 130-138.
4. Kedl, D. M., "Using a Two Dimensional Winding Model to Predict Wound Roll Stresses that Occur Due to Circumferential Steps in Core Diameter or to Cross-Web Caliper Variation," *Proceedings of the First International Conference on Web Handling*, May 1991.
5. Good, J. K., "Winding and Unwinding Webs: A Review of the State of Science in 2005," *Proceedings of the Eighth International Conference on Web Handling*, June 2005.
6. Forrest, A. W., "Wound Roll Stress Analysis Including Air Entrainment and The Formation of Roll Defects," *Proceedings of the Third International Conference on Web Handling*, June 1995, pp. 113-133.
7. Catlow, M. G. and Walls, G. W., "A Study of Stress Distributions in Pirns," *Journal of Textile Institute* Part 3, pp. T410-429, 1962.

8. Altmann, H. C., "Formulas for Computing the Stresses in Center-Wound Rolls," *Tappi Journal,* Vol. 51, No. 4, pp. 176-179, April 1968.
9. Yagoda, H. P., "Integral Formulas for Wound Rolls," *Mechanics Research Communications*, Vol. 7, No. 2, pp. 103-112, 1980.
10. Willett, M.S. and Poesch, W. L., "Determining the Stress Distributions in Wound Reels of Magnetic Tape Using a Nonlinear Finite-Difference Approach," *Journal of Applied Mechanics*, Vol. 55, pp. 365-371, June 1988.
11. Hoffecker, P. and Good, J. K., "An Axisymmetric Finite Element Model for Center Winding Webs," *Proceedings of the Eighth International Conference on Web Handling*, 2005.
12. Pfeiffer, J. D., "Internal Pressures in a Wound Roll," *Tappi Journal*, Vol. 49, No. 8, pp. 342-347, August 1966.
13. Boutaghou, Z. E. and Chase, T. R., "Formulas for Generating Prescribed Residual Stress Distributions in Center Wound Rolls," ASME Journal of Applied Mechanics, Vol. 58, pp. 836-840, September 1991.
14. Chandrupatla, T. R. and Belegundu, A. D., Introduction to Finite Elements in Engineering, 3rd edition, Prentice Hall, 2002, pp. 208-210.
15. Szilard, R., Theory and Analysis of Plates, Prentice Hall, 1974, pp. 375-376.
16. Cheng, S. and Cheng, C. C., "Relation between E, ν, and G and Invariants of the Elastic Coefficients for an Orthotropic Body," Mechanics of Wood and Paper Materials, ASME, AMD-Vol. 112, MD-Vol. 23, 1990, pp. 63-65.
17. Callister, W. D., Materials Science and Engineering an Introduction, 5th edition, John Wiley and Sons, Inc, 2000, pp. 792-796.

18. Timoshenko, S. P., Theory of Elastic Stability, McGraw-Hill Book Company, 1961, pp. 458.

APPENDIX

Test 1	6 inch	
Pile Height	MD	CMD
1.022	2	0
1.3475	-431	49
1.661	-500	73
1.93	-524	76
2.184	-524	77
2.436	-526	76

Test 2	6 inch	
Pile Height	MD	CMD
1.288	0	-1
1.506	-695	139
1.796	-820	172
2.186	-846	178
2.334	-849	180
2.563	-848	179

Test 3	6 inch	
Pile Height	MD	CMD
1.205	-1	0
1.52	-696	109
1.807	-816	121
2.087	-870	147
2.333	-895	148
2.571	-848	145

Test 4	24 inch	
Pile Height	MD	CMD
1.813	0	0
2.073	-585	160
2.31	-691	208
2.557	-717	225
2.802	-723	227
3.01	-724	237

Test 5	24 inch	
Pile Height	MD	CMD
1.872	1	-2
2.05	-618	154
2.305	-769	198
2.547	-745	212
2.772	-750	221
2.988	-752	221

Test 6	6 inch	
Pile Height	MD	CMD
1.215	-2	-1
1.535	-656	228
1.833	-788	257
2.0975	-813	261
2.357	-816	261
2.587	-818	260
2.821	-817	261
3.041	-815	259

Test 7	24 inch	
Pile Height	MD	CMD
2.0795	-2	-2
2.318	-442	23
2.567	-573	65
2.799	-617	77
3.009	-631	83
3.223	-639	88
3.414	-639	86
3.613	-638	84

Test 8	6 inch	
Pile Height	MD	CMD
1.215	5	-11
1.542	83	570
1.808	-62	594
2.089	-114	587
2.331	-127	590
2.5815	-131	572
2.806	-140	571

Test 9	6 inch	
Pile Height	MD	CMD
1.453	4	-13
1.744	-1752	457
2.022	-1922	451
2.28	-1936	351
2.52	-1963	350
2.752	-1964	352
2.981	-1969	354
3.189		351

Test 10	6 inch	
Pile Height	MD	CMD
1.346	-20	-3
1.654	-325	602
1.931	-458	649
2.198	-490	643
2.432	-501	636
2.67	-501	629
2.891	-500	623

Test 11	6 inch	
Pile Height	MD	CMD
1.439	12	-6
1.752	-676	331
2.03	-847	359
2.276	-892	357
2.512	-917	359
2.76	-920	361

Test 12	6 inch	
Pile Height	MD	CMD
1.431	-7	-15
1.746	-408	257
2.015	-577	280
2.269	-612	287
2.506	-622	270
2.742	-623	274

Test 13	6 inch	
Pile Height	MD	CMD
1.195	-12	-4
1.513	-660	508
1.8	-789	560
2.063	-820	568
2.32	-864	569
2.555	-878	571

Test 14	6 inch	
Pile Height	MD	CMD
1.746	-2	-9
2.021	-338	795
2.288	-534	816
2.531	-589	780
2.765	-633	792
2.992	-572	706
3.189	-615	688

Test 15	6 inch	
Pile Height	MD	CMD
1.392	-4	4
1.701	-472	322
1.98	-582	367
2.244	-620	376
2.483	-637	380
2.718	-641	381
2.936	-646	380

Test 16	6 inch	
Pile Height	MD	CMD
1.448	-7	3
1.74	-963	276
2.016	-1150	328
2.268	-1190	340
2.508	-1204	344
2.74	-1200	349
2.954	-1205	350

Test 17	6 inch	
Pile Height	MD	CMD
1.731	-8	-11
1.996	-978	424
2.31	-1206	441
2.546	-1230	465
2.781	-1249	425
2.987	-1215	427
3.193	-1215	417

Test 18	24 inch	
Pile Height	MD	CMD
1.58	-2	3
1.869	-476	191
2.135	-596	244
2.378	-617	264
2.632	-636	272
2.846	-633	270
3.061	-633	270

Test 19	24 inch	
Pile Height	MD	CMD
1.631	-2	0
1.918	-284	228
2.167	-398	309
2.405	-430	342
2.63	-434	346
2.866	-439	350
3.077	-440	348

Test 20	24 inch	
Pile Height	MD	CMD
1.688	-2	-1
1.966	-349	362
2.223	-464	442
2.47	-497	476
2.699	-501	489
2.912	-506	487
3.134	-503	487

VITA

Angela De'on Welch

Candidate for the Degree of

Master of Science

Thesis: STUDY ON THE DEVELOPMENT OF AXIAL STRESSES IN WOUND ROLLS

Major Field: Mechanical Engineering

Biographical:

Personal Data: Born in Sayre, Oklahoma on December 17, 1976, the daughter of Phil and Regina Barker.

Education: Graduated from Sapulpa High School, Sapulpa, Oklahoma in May of 1995; received Bachelor of Science degree in Mechanical Engineering from Oklahoma State University, Stillwater, Oklahoma in May of 2004; completed the requirements for the Master of Science degree with a major in Mechanical Engineering at Oklahoma State University in December of 2006.

Experience: Worked as a Co-op Engineer at American Airlines in Tulsa, Oklahoma from January 2002 to August 2002, Fall of 2003 and January 2004 to July 2004; employed by Oklahoma State University as a graduate teaching assistant in Fall of 2004 and Spring of 2005 and as a graduate research assistant from Summer 2005 to present.

Professional Memberships: Society of Women Engineers

Name: Angela De'on Welch Date of Degree: December, 2006

Institution: Oklahoma State University Location: Stillwater, Oklahoma

Title of Study: STUDY ON THE DEVELOPMENT OF AXIAL STRESSES IN WOULD ROLLS

Pages in Study: 91 Candidate for the Degree of Master of Science

Major Field: Mechanical Engineering

Scope and Method of Study: The primary objectives for this thesis were to establish if the axial stresses that are associated with winding are sufficient to cause corrugation failures and to verify if a two-dimensional winding model accurately predicts the stresses seen in a roll that were obtained experimentally. In order to validate the model, machine direction and cross machine direction strains were measured experimentally during the winding process. Two different widths of web were tested, a 6 inch wide web and a 24 inch wide web. Model stresses were converted to strains and a comparison was made between the experimental strains and the model strains.

Findings and Conclusions: The two-dimensional model used made a good prediction of machine direction strains when compared with the experimental results. This agreement was made possible by adding a negative bending strain value to the machine direction strains that were obtained experimentally. The model was verified with the cross machine directions strains for the 24 inch wide web, but not the 6 inch wide web. The 24 inch wide web was approaching a plane strain condition; therefore the model is verified for conditions where plane strain conditions exist. A conservative critical axial stress equation was used to aid in predicting corrugation failures in the roll. According to the equation, corrugations should have appeared in the 24 inch roll, but not the 6 inch roll. When performing experiments, corrugations were not observed in either width of roll. The critical axial stress equation used did not account for the stiffness of the web material that was supporting the outer layer of the wound roll, explaining why corrugations were not seen.

ADVISER'S APPROVAL: J. K. Good